Clim Dyn (2011) 36:845–866
DOI 10.1007/s00382-010-0820-4

Synoptic conditions of extreme windstorms over Switzerland in a changing climate

Stéphane Goyette

Received: 1 July 2009 / Accepted: 10 April 2010 / Published online: 23 April 2010

Abstract This paper reports on a method using composites for studying synoptic conditions of a series of windstorm events selected on the basis of maximum wind speeds in Switzerland. The composite storm-averaged conditions indicate how flow fields, as well as related surface conditions, are organised so as to produce high wind speeds near the surface. On average, high winds in Switzerland, mainly generated by transient synoptic-scale eddies, are characterised by a minimum in the mean sea level pressure field over southern Norway, anticyclonic conditions south of 35°N and a steep pressure gradient over continental western Europe. The geopotential aloft has a predominant zonal structure, producing high winds between 45°N and 50°N over the eastern Atlantic and further inland; the jet stream has its maximum speed at 50°N over the Celtic Sea and Brittany at 250 hPa. Close to the surface, large temperature contrasts between the warm waters of the Atlantic Ocean and Mediterranean Sea and the cooler continent are diagnosed. The results thus obtained differ to those produced by other methods based on the analysis of deep cyclones or of strong vorticity in the northern North Atlantic Ocean basin. Differences of the composite mean synoptic conditions for current (1961–1990) and future climate (2071–2100) as simulated by the Global Climate Model HadAM3H in the context of the EU PRUDENCE project indicate that windstorms in a warmer world are generated by a subtle modification of the atmospheric baroclinicity, especially over the ocean and where greater ocean-continent temperature contrasts are simulated during winters. However, there are no signs of reduced storm activity as the climate warms by the end of the twenty-first century.

S. Goyette (✉)
Climatic Change and Climate Impacts, University of Geneva, 7 route de Drize, Geneva, Switzerland
e-mail: stephane.goyette@unige.ch

1 Introduction

Storms associated with extratropical cyclones assume a large variety of forms depending on the background flow in which they are embedded (Holton 2004). Deep cyclones may produce strong pressure gradients and have the potential to induce severe weather, characterised by their high winds over maritime and continental areas (e.g., von Storch and Weisse 2008). The consequences of global warming caused by the increase of greenhouse gases in the atmosphere on the passage of cyclones in the North Atlantic, and its impacts over Western Europe, is a matter of continuous analysis and investigation (Beniston et al. 2007; Fuhrer et al. 2006; Leckebusch et al. 2006). Some studies report an intensification in the storm climate in the North Atlantic from the mid 1970s to the mid 1990s (Schmith et al. 1998); that positive trend may well continue or not in the future (Fischer-Bruns et al. 2005; Bengtsson et al. 2006). The storm climate in northern Europe has been apparently stable over the last centuries in which inter-decadal variability is an inherent feature of the storm activity. Even though the positive trend in NW Europe started in the 1960s has apparently been broken (e.g., Alexandersson et al. 2000), the present intensity of the storm and ocean wave climate seems to be comparable with that at the beginning of this century (Bärring and von Storch 2004). In a recent study by Wang et al. (2009), using the data of the latter, storminess is displaying strong differences between winter and summer, and between the North Sea area and other parts of the northeast North Atlantic region. In particular, winter storminess showed an

unprecedented maximum in the early 1990s in the North Sea area and a steady upward trend in the northeastern part of the region, while it appears to have declined in the western part of the region. Part of this phenomenon is found to be related to the North Atlantic Oscillation (NAO); apparently it has not gone beyond the bounds of natural variability (WASA group 1998). It is well recognised that the NAO influences the changes of surface westerlies across the North Atlantic into continental areas (Stephenson et al. 2002). Global warming may have an influence on the upward trend and the spatial pattern shift on the winter NAO (Osborn et al. 1999; Ulbrich and Christoph 1999), but this issue is still not yet quite clear (Pinto et al. 2009; Stephenson et al. 2006). At present, the understanding of current and future changes in extratropical storm activity is a matter of great interest; studies are still not clear about the issue of future storms in the North Atlantic Ocean in terms of their tracks, frequencies and intensities, as well as their further impact inland (Ulbrich et al. 2009; Raible et al. 2008; Lambert et al. 2002; Leckebusch and Ulbrich 2004).

The variation of storm activity in a changing climate is related to the alterations in the mean atmospheric flow fields. The enhancement of atmospheric greenhouse gases can lead to a number of potential changes which may affect storm activity; observational analysis (Wang et al. 2006) as well a number of studies show that there is a poleward shift in storm activity (Fischer-Bruns et al. 2005; Knippertz et al. 2000). Some noticeable changes are also found in cyclone life cycle characteristics (Löptien et al. 2008). The total number of cyclones would not apparently change significantly in a warmer climate but cyclone frequencies and intensities may vary regionally. Many studies even suggest a reduction of the total number of cyclones under future climate conditions (e.g., Lambert and Fyfe 2006; Ulbrich et al. 2009). On the one hand, the cyclone climatology change signal shows a large variability and important differences across European regions but number of cyclones presumably decreases in future conditions throughout Europe (Lionello et al. 2008). On the other hand, while the total number of cyclones may be reduced, the number of extreme cyclones affecting Western and Central Europe may increase (Ulbrich et al. 2009; Della-Marta and Pinto 2009, among others). The decreased horizontal temperature gradient in the lower troposphere in winter, leading to a reduction of the baroclinicity, should lead to a reduced intensity of extratropical storm activity (Branscome and Gutowski 1992; Hall et al. 1994; Carnell and Senior 1998). An increase of baroclinicity in the upper atmosphere (Land and Feichter 2003), may lead to an increase in extratropical storm activity. The net effect of temperature change on the occurrence and intensity of cyclones, and on the low-level wind speed, is thus still not clear. However, baroclinic wave activity is presumably more sensitive to lower level change which could lead to a reduced baroclinicity in the low levels in addition to an enhancement of baroclinicity by the reduced vertical static stability which would presumably lead to a poleward shift of the of greatest baroclinic instability (Held 1993). Pinto et al. (2009) diagnosed that the enhanced number of extreme cyclones in positive NAO phases can be explained by the larger area with suitable growth conditions, which is better aligned with the cyclone tracks and is associated with increased cyclone life time and intensity. Their results shown similar behaviour for future climate conditions (SRES A1B scenario), but a small increase of the frequency of extreme values is detected near the cyclone cores. On the other hand, total cyclone numbers decrease by 10% over the North Atlantic with an exception is the region near the British Isles. Using a high resolution GCM (spectral T163) with the same emission scenario, Bengtsson et al. (2009) concluded for a small reduction in the number of cyclones but no significant changes in the extremes of wind and vorticity. However, cyclones would move toward the southern and eastern coast of Greenland but the strongest winds would be found around the coasts and between Greenland and Iceland. They mentioned that the reason for this is not straightforward but it maybe related to a greater preference for the storm tracks to be orientated toward the British Isles and Scandinavia and a corresponding weakening both to the North and to the South. As hypothesised in Bengtsson et al. (2006), this may be related to an enhanced SST gradient between 40° and 50°N in the central Atlantic with associated increase in baroclinicity. It has also been hypothesised that storm activity in a warmer world could increase in response to larger land-sea temperature contrasts (Houghton 2005).

Extra-tropical storm activity may be analysed using a variety of methods and indices. An observational and theoretical overview of mid-latitude winter storm tracks is found in Chang et al. (2002). For example, the meridional temperature gradient indexes the temperature contrast across mid-latitudes that is related to extratropical eddy activity (Gitelman et al. 1997). Iskenderian and Rosen (2000) propose an index of cyclone activity based on the temperature variability at 500 hPa. Cyclone activity is closely related to the large-scale baroclinicity of the atmosphere. A suitable measure of the baroclinicity is provided by the Eady growth rate (Hoskins and Valdes 1990). The storm tracks have been defined as region of maximum standard deviation of a chosen geopotential level (e.g., Blackmon 1976; Serreze 1995). Storms can be characterised by their changes in frequency and/or change in core pressure by counting the number of cyclones in a domain (e.g., Schinke 1993; Gulev et al. 2001), their dimensions (Rudeva and Gulev 2007; Nielsen and Dole

1992), their deepening rate in order to identify explosive cyclones (Sanders and Gyakum 1980; Roebber 1984), or by their weather impacts such as precipitation (Chang and Song 2006), wind speed (e.g., Rockel and Woth 2007; Zwiers and Kharin 1998), surges (e.g., Woodworth and Blackman 2002), and return periods for minimum central pressure and maximum vorticity such as in Della-Marta and Pinto (2009). Ulbrich et al. (2001) analysed the stormy December 1999 month and concluded that extreme winds were produced by a family of cyclones where high baroclinicity near the cyclone track over the eastern North Atlantic and extending partly into Europe was a major factor, and Wernli et al. (2002) analysed the December 1999 storm Lothar from a potential vorticity perspective. Storm Kyrill that swept across Western, Central, and Eastern Europe in mid-January 2007, whose development and impacts are described in Fink et al. (2009), has been analysed in terms of synoptic as well as by mesoscale conditions to explain the maintenance and intensity of this storm. Raible et al. (2007) concluded that the temperature gradient and the lower tropospheric baroclinicity help in the intensification of extreme cyclones in the Maunder Minimum simulations. Raible (2007) stated that during winter, changes in the meridional temperature gradient, the land-sea temperature contrast, and to some extent changes in static stability modulate the lower to middle tropospheric baroclinicity, being important in the intensification process. Leckebusch and Ulbrich (2004) identified cyclone systems using an algorithm based on the search for the maxima of the Laplacian of the mean sea level pressure and concluded that for an increase of the track density and a tendency for more intense systems over western Europe as climate warms. Although some overall agreement is found in the results produced by a number of such approaches, spatial and temporal behaviour of the results may vary significantly (Paciorek et al. 2002). For instance, Ulbrich et al. (2009) in their review paper shown that some results of cyclone related studies may seem to disagree even when based on identical data. Reasons for this are the variety of approaches for cyclone studies, starting from their identification and tracking and ending at the intensity measures. Consequently, their conclusions stated that investigations of cyclones should be approached by different means rather than by simple standard diagnostics. In most studies, baroclinicity is diagnosed through the growth rate of fastest growing Eady wave and thus measures the susceptibility of the basic state to baroclinic instability (Lindzen and Farrel 1980; Hoskins and Valdes 1990).

Schiesser et al. (1997) concluded to a decreased in the frequency of severe storm over northern Switzerland since about 1880; however, they used only four station observations. Consequently, if one is interested in the local impact of extra-tropical storms over a country or a region of interest in a changing climate, other approaches are needed. Nowadays, a focus is made on extreme weather conditions associated with extra-tropical storms because damages caused by high winds and gusts experienced near the surface may exceed the hazards related to climate warming itself (Kunkel et al. 1999; Munich Re 1999). Our understanding of how cyclones and windstorms over a region of interest would respond to climate change is rather rudimentary. What we need to understand, in particular, are the synoptic-scale conditions conducive to windstorms over a region, i.e., why and how these may change if climate is warming.

Consequently, the goal of this paper is to analyse the change of synoptic conditions conducive to extreme windstorms in Switzerland as a result of global warming conditions. A methodology is thus proposed whereby synoptic conditions of deep cyclones aggregated into composites for current, as well of those for future climate are analysed on the basis of the maximum wind speed generated over Swiss territory. A composite diagnosis of synoptic-scale extratropical cyclone development has been performed over the United States (Rolfson and Smith 1996). Their results have shown some of the mechanisms responsible for cyclone developments and weakening stages using the Zwack-Okossi equation (Zwack and Okossi 1986), but only few different cases were analysed and a generalisation to conditions generating windstorms is not possible.

In the present study, the use of a physically based tool such as a Regional Climate Model (RCM) is motivated for a number of reasons. Actually, RCM technology allows downscaling global reanalyses as well as GCM outputs for selected storms. Using this dynamic downscaling technique, the impacts of storms on the generation of high winds in Switzerland are analysed on a case-by-case study basis. Analysis of results is carried out using common basic diagnostics on a common grid which make possible and ease the intercomparison. In addition to the commonly used growth rate of fastest growing Eady wave, the vertical component of the baroclinicity vector is also employed; it is a member of the vorticity tendency equation and represents the generation of the vorticity which is necessary for cyclone amplification.

2 Methodology

Regarding its impact, wind speed represents an optimal parameter for selecting storm events in this investigation. The reason for this is related to the many hazards and the resulting damage which are directly (e.g., forest damage), or indirectly (e.g., economic repercussions), related to it (Weisse et al. 2005). Consequently, synoptic conditions of

extreme storms over Switzerland are determined on the basis of wind speeds. The methodology requires both observations of past climate and model simulations of current climate and climate change, and a numerical model to downscale these storms on a common grid to produce composites for which analysis is performed.

The first step aims at selecting the storm events. Windstorms are identified on the basis of the strongest "local" wind speeds. Wind observations are coming from the Swiss National Automatic Meteorological Network [see the CLIMAP (weather and climate data the Swiss national weather service available at: http://www.meteoschweiz.ch/web/en/services/data_portal/climap-net.html)] for a number of stations (approx. 70) from 1978 onwards which are then averaged and sorted out in decreasing order of magnitude. The other source of is coming from the Danish Meteorological Institute 50-km HIRHAM Regional Climate Model simulated winds available in the context of the EU 5th framework Program PRUDENCE (Christensen et al. 2002) over two periods, 1961–1990 using prescribed greenhouse gas forcing based on observations, and 2071–2100 for the purposes of the SRES A2 greenhouse gas emission scenario (Nakićenović et al. 2000) provided by the Web site http://prudence.dmi.dk/. These wind speeds are then averaged at the 21 HIRHAM grid points covering Switzerland and also sorted out in decreasing order of magnitude.

The second step aims at selecting the synoptic conditions corresponding to these storms for the current and future simulated climates. Reanalysis data and those coming from Global Climate Model simulated outputs are then compiled to form three sets of composites. The quantities are coming from two main sources: (1) NCEP-NCAR reanalysis provided by the NOAA/OAR/ESRL PSD, Boulder, Colorado, USA, from their Web site at http://www.cdc.noaa.gov/, (2) Hadley Centre HadAM3H GCM (HCGCM) outputs, obtained in the context of the EU 5th framework Program PRUDENCE (Christensen et al. 2002) over two periods 1961–1990, and 2071–2100 under the A2 greenhouse gas emission scenario, that also served to drive the HIRHAM RCM cited above, provided by the Web site http://prudence.dmi.dk/.

The third step uses a Regional Climate Model to downscale these synoptic conditions selected in the second step. A common computational setup employs a common grid, a common archival frequency, and a common set of variables for the analysis in order to project all these storms over a fixed period of time. The model used in this study is the Canadian RCM (CRCM) whose principal characteristics are an efficient semi-Lagrangian, and a semi-implicit marching scheme (Tanguay et al. 1990; Laprise et al. 1997), interfaced with the physical parameterizations of the second generation GCM of the Canadian Centre for Climate modelling and analysis (GCMii; Mcfarlane et al. 1992). A few upgrades were added, such as a modified cloud onset function (Caya and Laprise 1999), and a multi-level large-scale nudging interface (Biner et al. 2000). This combination is used for both short- and long-term applications (Caya and Laprise 1999; Laprise et al. 1998).

Finally, the fourth step carries out analysis of the results of the storm composites produced by the CRCM in order to study and compare synoptic conditions conducive to windstorms over the Swiss territory. To assess the cyclonic activity in the North Atlantic basin, as well as its impact over the European continent, a number of fields and diagnostics are considered. The quantities of interest are namely the mean sea level pressure, p_{msl}, the geopotential, Φ, the 1,000–500 hPa thickness, the specific humidity, q, the temperature, T, the vertical component of the relative vorticity, $\boldsymbol{\zeta} = \hat{\mathbf{k}}(\nabla \times \boldsymbol{V})$, in which the wind velocity vector is $\boldsymbol{V} = [u, v, w]$, where u, v, w represent, respectively, the West-East, the South-North and the vertical wind components in the local Cartesian coordinate system and $\hat{\mathbf{k}}$ a local unit vector positive upward, the divergence, $D_{\mathrm{H}} = \vec{\nabla}\boldsymbol{v}_H$, where $\boldsymbol{v}_{\mathrm{H}} = [u, v]$ is the horizontal wind speed components of magnitude $v_H = (u^2 + v^2)^{1/2}$, and the precipitation, P.

The evolution of strong storm systems is thought to depend on the baroclinic instability of the atmosphere. A measure of baroclinicity is the maximum Eady growth rate (Lindzen and Farrell 1980), defined as:

$$\sigma_{\mathrm{BI}} = 0.31 \frac{f}{N} \left| \frac{\partial v_{\mathrm{H}}}{\partial z} \right| \tag{1}$$

where f is the Coriolis parameter, N the Brunt–Väisälä frequency, and z is the vertical component of the local Cartesian coordinate system. The parameter was also used to study the maintenance of winter storm tracks by Hoskins and Valdes (1990).

While former studies focus primarily on the Eady growth rate as a diagnostic quantity to the baroclinicity of the atmosphere, this paper considers the baroclinicity vector $\boldsymbol{N} = -\nabla T \times \frac{R}{p}\nabla p$, where p is the pressure, and R the gas constant for air. Given that large-scale atmospheric motions are predominantly horizontal, the vertical component of the baroclinicity vector is retained, namely $N_z = -\hat{\mathbf{k}}\boldsymbol{N}$. Since we are describing synoptic conditions on pressure levels, we can use the hydrostatic approximation combined with the ideal gas law to rewrite this component as follows:

$$N_z = \frac{\partial \ln T}{\partial y}\frac{\partial \Phi}{\partial x} - \frac{\partial \ln T}{\partial x}\frac{\partial \Phi}{\partial y} \tag{2}$$

where x and y represent, respectively, the West-East and the South-North components of the local Cartesian coordinate system. In synoptic applications, the T surfaces and the Φ surfaces intersect in space defining a continuous

family of solenoids, and the number per unit area measures the degree of baroclinicity (Peixoto and Oort 1991; Chap 3).

2.1 Windstorm identification

In order to provide for a statistically significant analysis, sets of thirty storms are considered on the basis of the hourly maximum anemometer-level wind speed over Swiss territory. Maximum hourly windspeeds are averaged across all of the available stations and the thirty most intense averages were taken into consideration. Averaging windspeed values over Switzerland, sorting the averages out by deceasing order of magnitude, and selecting the first members in the list is a particular way to "filter out" the strongest country-wide storms. It thus aims to avoid marginal storms that swept parts of the country and also tries to discard thunderstorms, which generally produce local wind maxima. Other methods exist and these are leading to roughly the same windstorms (not shown). The most important aspect of the methods to be used here is that these pick those particular cyclones responsible for strong winds in Switzerland no matter how the strongest are ranked in the list since statistics of the composites are analysed. It is true that one should not overweight stations at exposed locations, but "major" storms, in the sense defined here, and over a small country such as Switzerland, have an imprint (i.e., a distinct wind maximum) on much of the wind records either at low or/and high elevations. The selection issue would have been of prime importance if only few storms were included in the composites, which is clearly not the case in this study. The first set corresponds to observed wind storms. The time coordinates of these are then sorted and the corresponding synoptic NCEP-NCAR reanalysis data is considered, namely: the air temperature, the specific humidity, the geopotential and the horizontal components of the wind velocity vector. These reanalysis data are available at 6-hourly intervals for the period 1958–2006 (Kalnay et al. 1996). The spatial resolution of this data is about 210 km × 210 km with 12 vertical levels (T62/L12) and is used as a surrogate for the "observed" synoptic conditions. The second and third sets correspond to simulated wind storms. HIRHAM simulated winds are used as the "fine-scale" winds over Swiss territory and serve to identify the storms whereas HCGCM outputs serve as "synoptic" conditions, and the thirty most intense averages are taken into consideration. A similar procedure to that described above was then carried out; the time coordinates of these wind storms were sorted and the corresponding synoptic HCGCM data available at 6-hourly was taken into consideration. This GCM has been used to drive HIRHAM as well as a number of other RCMs in the context of the PRUDENCE project, and it compares well with observed surface pressure, temperature and other flow fields (Beniston et al. 2007).

The averages of these three storm composites are then suited to the analysis of the synoptic conditions over the computational domain (as shown in Fig. 1).

2.2 CRCM simulation setup

For the current application, the computational domain is a north polar stereographic grid centred over the Bay of Biscay off the west coast of France (46°N; 5°E). The mesh has a 150 km grid spacing and twenty vertical levels. The relatively coarse grid spacing in the horizontal, still finer than that of the reanalysis and that of the HCGCM, is adequate to carry out synoptic analyses for which the length scale for midlatitude synoptic systems. Lateral and upper boundary atmospheric conditions are provided by NCEP-NCAR reanalysis data and by the HCGCM outputs. The nudging procedure forces the model towards the large-scale flow over the computational domain as prescribed from NCEP-NCAR reanalysis data, and from previously-simulated runs with HCGCM outputs. The observed sea-surface temperature and sea-ice are taken from the available information provided by the AMIP project (Taylor et al. 2000). Simulated data is provided by the UK HADLEY Centre HadAM3H global model (Pope et al. 2000) which also provide for sea-surface temperature and sea-ice derived from observations in the 1960–1990 period, and with UK HADLEY Centre HadCM3 SST and sea-ice anomalies added for the scenario integration. Surface fields of soil, land use, vegetation types and other physiographic characteristics are prescribed from the Wilson and Henderson-Sellers (1985) datasets.

Each simulation runs over a nine-day period centred on the day of the wind maximum identified in the wind observations and in the HIRHAM wind outputs. This period is short enough to warrant a fast computational turnaround but sufficiently long to avoid spin-up problems in the flow and the surface fields (e.g., Goyette et al. 2001). The archival frequency is three-hourly. The synoptic conditions producing windstorms over Switzerland are chosen as these corresponding to the time of the strongest simulated maximum wind speed over the Swiss territory. The three sets of thirty storm composites are thus made on the basis of those conditions.

A favourable comparison of the "current" observed and simulated conditions would indicate, with some confidence, that the current simulated cyclonic activity and the storms in a future warmer world would be reproduced realistically. Subsequently, differences in the simulated storm statistics between the period 2071–2100 and those of the period 1961–1990 are analysed on a grid-point basis. To assess the degree of significance of the differences in the composite

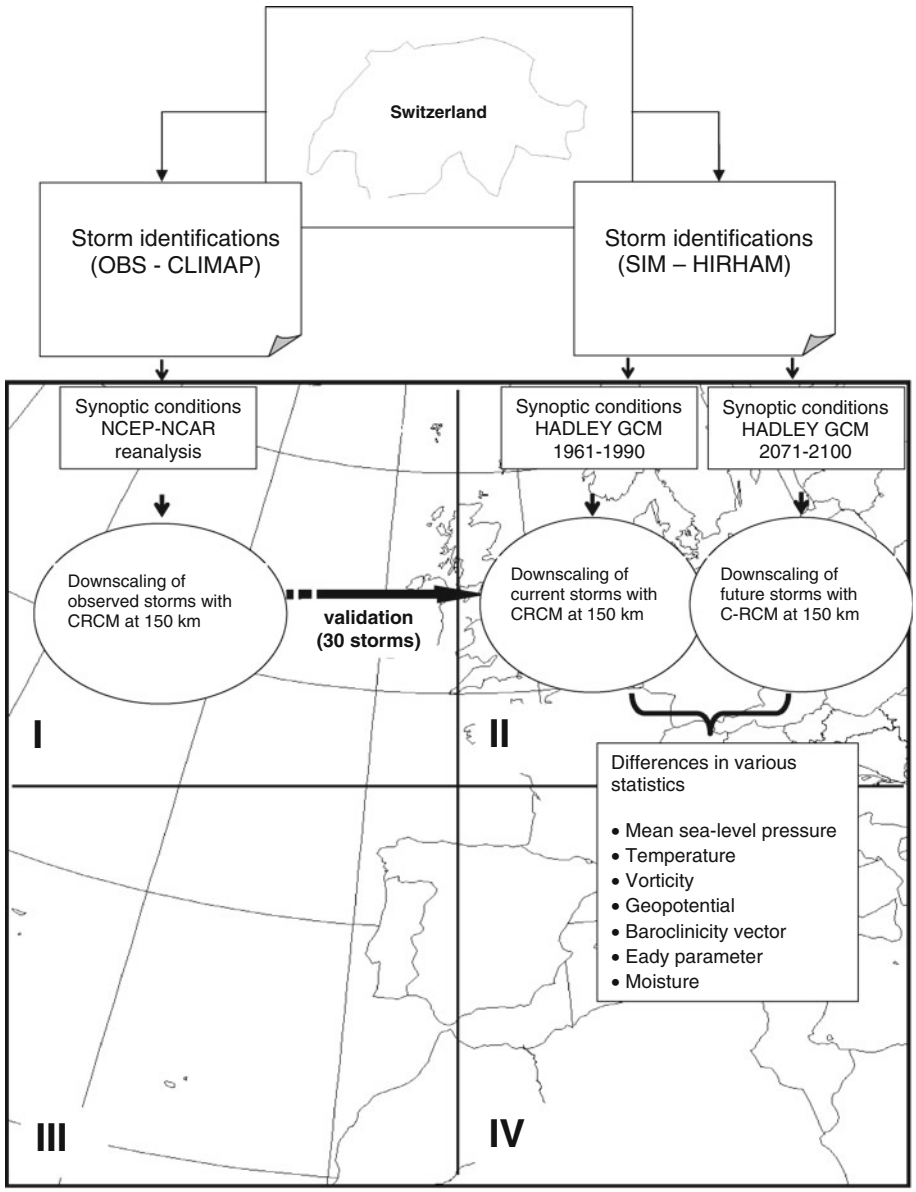

Fig. 1 Schematic diagram of the many steps followed in the methodology of the evaluation of synoptic conditions of windstorms in a changing climate. These include the storm identification at the Swiss level to the downscaling of individual events using a RCM on the computational domain shown above. This domain of approximately 5,000 km × 5,000 km is partitioned into four quadrants further used in the synoptic analysis. Acronyms and symbols are defined in the text

distributions, Student's *t* test assesses whether the means of two sets are statistically different from each other. Also, the non-parametric Kolmogorov–Smirnov and Mann–Whitney tests are used to estimate whether or not the two sets may be reasonably assumed to come from the same distribution (e.g., Wilks 2006).

3 Results

A validation step is carried out to verify whether or not the HCGCM reproduce the current observed conditions (i.e., NCEP-NCAR) leading to extreme winds over Switzerland realistically during the period 1961–1990. This is done by comparing the first two composite distributions, i.e., the synoptic conditions averaged over the "30" most intense storms from the NCEP-NCAR atmospheric data compared to the "30" most intense storms simulated by the HCGCM over the period 1961–1990, both downscaled with the CRCM. The comparison and the analysis are performed on a common diagnostic grid.

3.1 Validation for current climate

The storm identification procedure identified the mother cyclones associated with the first two major windstorms that struck Switzerland, namely the 26 December 1999 "Lothar" and the 27 February 1990 "Vivian" storms, which are formally members of the observed composite. Some other storms included in the composite have also

been referenced. Two members of the composite based on observations are shown in Fig. 2 in terms of their mean sea level pressures, 500 hPa geopotential heights, 1,000 hPa winds, and precipitation rates, including the Vivian storm (Schüepp et al. 1994) and the January 1994 storm that struck the UK, Germany and Switzerland (reported in Heneka et al. 2006). Figure 2 shows to some extent that the variability of the mean sea level pressure and that of the 500 hPa geopotential height is found in the upper half of the computational domain (in quadrants I but also in II). The windspeed values are more variable over the ocean, and the precipitation rate maximum may be found North of Switzerland whose variability decreases almost symmetrically away from that centre. Generally, the CRCM lowest level maximum windspeed simulated during the period is reproduced within a period of 6 h compared to the observations. The observed and simulated storms considered here are induced by deep cyclones travelling across the North Atlantic Ocean. Observations show that the months during which intense storms prevail extend from October to March, peaking in December with 33% of the total; simulated outputs show a similar storm distribution. In Table 1, the minimum, maximum, mean, and standard deviation values of the mean sea level pressure for each individual storm as well as these for the composites, and the statistics indicate that the simulated p_{msl} conducive to windstorm over the Swiss territory are reproducing the mean NCEP-NCAR conditions well; (1,012.5 vs. 1,012.0 hPa) for the composite mean p_{msl} (1,001.7 vs. 1,002.5 hPa) for the composite minimum p_{msl} (1,021.7 vs. 1,020.6 hPa) for the composite maximum p_{msl}, despite a positive biases, up to 7 hPa, in the minimum and maximum pressure found on the computational grid. The spatial distributions of the composites averages generated with HCGCM (1961–1990) are similar to that observed despite some details as shown in Fig. 3a–d, and described next. The correspondence between the patterns found in the composites is depicted in Table 2, where the spatial linear correlation coefficient between two similar fields show how the HCGCM storm composite downscaled by the CRCM for the period 1961–1990 reproduced that of the NCEP-NCAR reanalysis for some selected vertical levels. The results analysed and shown below are thus the composite field averages of thirty storms of the NCEP-NCAR and simulated current (1961–1990) conditions scaled by the CRCM. The fields shown next are smoothed using a first-order two-dimensional linear filtering scheme in order to facilitate visual examination and aid interpretation.

Figure 3a shows the composite mean p_{msl} fields; they are both characterised by a pressure centre of less than 990 hPa located over southern Norway and a high pressure region covering Portugal, southern Spain and Morocco producing a strong pressure gradient over northern France and over the English Channel along the 50th parallel. Over Switzerland, it is roughly 4 hPa across the country. The geopotential height field at 500 hPa (not shown) is characterised by a meridional structure with a trough above the 50°N centred between 10°W and 10°E, along with a steep slope creating strong gradient of geopotential height over western Europe. Figure 3b shows the 1,000–500 hPa characterised by thickness values of 560 dam to the south and 525 dam to the north, a difference of 615 m in the computational domain. Surface temperatures are characterised by warm waters in the Atlantic and Mediterranean and colder temperatures inland, thus creating steep water-continental temperature gradients, as shown in Fig. 3c. The main feature of the precipitation field is a region of heavy precipitations centred over Luxembourg at 8.7 mm day^{-1} (Fig. 3d).

In the following composite mean profiles are compared the simulated quantities for the period 1961–1990 against the NCEP-NCAR reanalyses. In order to show some of the spatial features found in the composites more clearly, the computational domain is partitioned into quadrants as displayed in Fig. 1, namely I (NW; mostly ocean), II (NE; mostly land), III (SW; mostly ocean), and IV (SE; half ocean-half land).

Wind speeds (1,000 hPa) over 14 m s^{-1} are found where the mean sea level pressure gradient is the steepest over northern France, Belgium and southern England, and where the direction is predominantly westward (not shown). As Leckebusch and Ulbrich (2004) noted, the average maximum surface wind speed is reached southwest of the tracks of cyclones; this is also the case here in the composites. At the 500 hPa level, a strip of wind over 30 m s^{-1} is also found over the North Atlantic Ocean 5° on both sides of the 50th parallel, and extending over Switzerland and Germany inland. A straight upper-level jet is found at 225 hPa characterised by winds propagating eastward in a narrow band 3° on both sides of 50°N from the North Atlantic (20°W), having a high speed core flowing eastward at $v_H > 45$ m s^{-1} over Brittany that produces averaged winds of more than 35 m s^{-1} as shown in Fig. 4a, flowing across France and reaching into Switzerland. Patterns found in the composites generated with HCGCM (1961–1990) wind fields are similar but underestimated by about 3 m s^{-1} on the vertical average in the atmospheric column.

The air temperature field is characterised by a strong meridional structure, but the effect of warm ocean currents flowing northeast is apparent in the lowest levels. The temperature at 1000 hPa has a strong zonal structure where a North-South gradient of more than 15°C can be seen in the computational domain. Similar patterns are also found in the composites generated with HCGCM (1961–1990), but a difference of up to 1°C is found over the ocean, and a cold bias (up to 2.5°C) over land. In the vertical, the

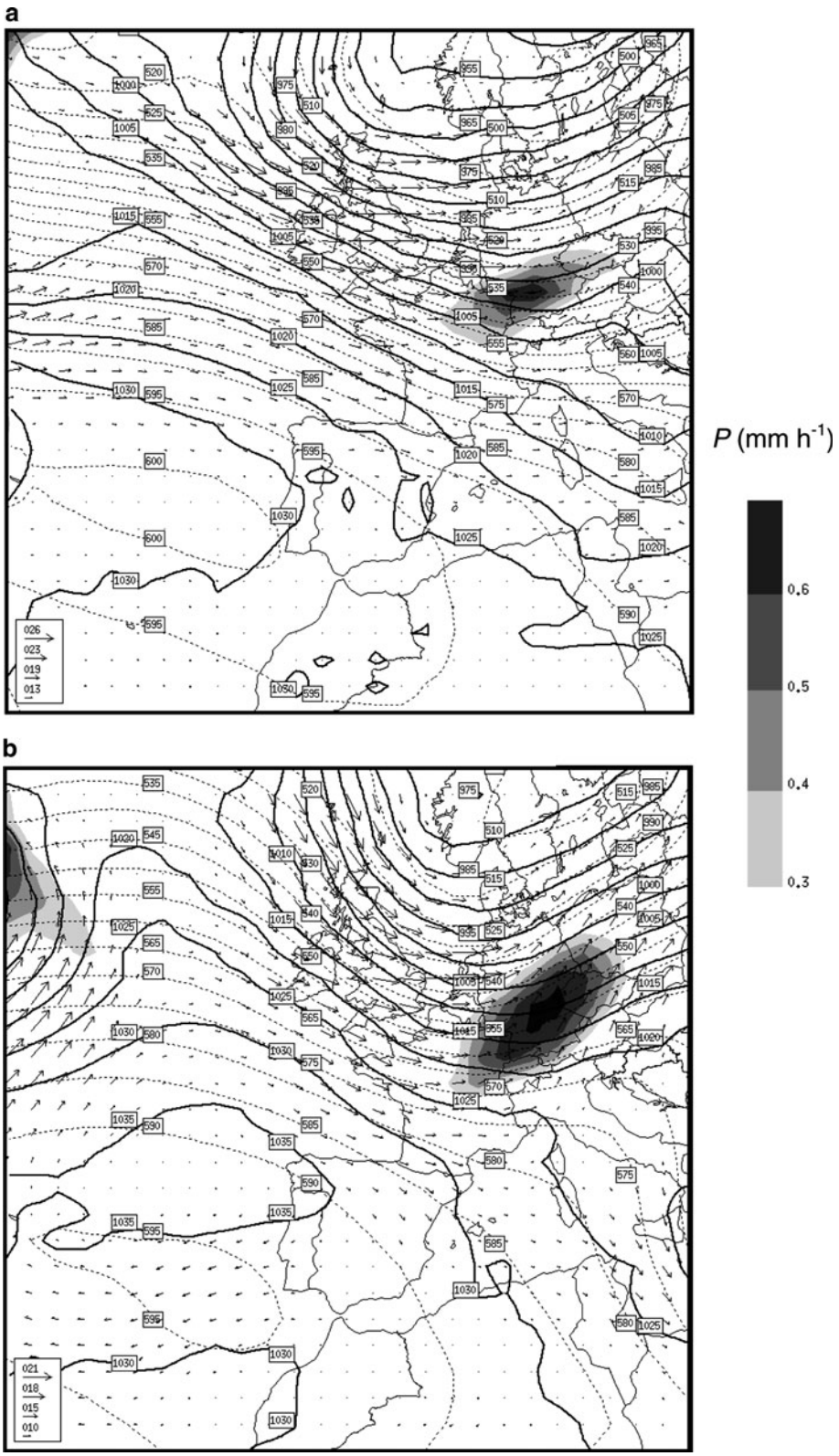

Fig. 2 Two members of the composite based on observations: **a** the 27 February 1990, 1200 UTC, and **b** the 28 January 1994, 1200 UTC storms. The precipitation rate is in *grey shades* with isohyets drawn every 0.1 mm h^{-1}, the p_{msl} in *solid black* with isobars drawn every 5 hPa, the 500 geopotential height in *dotted grey* with contour lines drawn every 5 dam, and the 1,000 hPa wind vectors in m s^{-1} with scales in *inserts*

simulated average temperature profile is overestimated by about 0.86°C in the column on average, and is more pronounced over the land (1.3°C) and less over the sea (0.3°C) as shown in Fig. 4b. Both observed and simulated thermal profiles are stable: this is a remarkable storm feature already noted during the storm-averaged profiles (Goyette 2008), as well as during the specific Lothar and Vivian storms (Goyette et al. 2003, Goyette et al. 2001).

Table 1 The mean sea level pressure statistics for all members of the three storms composites where the minimum, maximum, mean and standard deviation values are evaluated on the computational grids

NCEP-NCAR					Hadley GCM 1961–1990				Hadley GCM 2071–2100			
Storm #	Min (hPa)	Max (hPa)	Mean (hPa)	Stdev (hPa)	Min (hPa)	Max (hPa)	Mean (hPa)	Stdev (hPa)	Min (hPa)	Max (hPa)	Mean (hPa)	Stdev (hPa)
1	978.9	1,030.1	1,006.3	12.6	977.7	1,040.5	1,013.9	12.8	971.2	1,036.0	1,010.6	13.3
2	973.5	1,032.9	1,012.9	15.8	981.0	1,040.4	1,008.4	12.8	993.6	1,042.6	1,016.6	8.6
3	979.2	1,029.3	1,010.8	14.3	990.4	1,039.1	1,019.9	10.9	971.0	1,037.6	1,001.8	15.6
4	975.8	1,028.8	1,007.6	16.1	988.8	1,032.2	1,015.9	9.2	979.1	1,033.8	1,003.3	11.0
5	971.6	1,032.4	1,011.6	17.0	982.7	1,047.0	1,016.0	12.7	978.6	1,041.8	1,007.1	13.8
6	977.3	1,030.4	1,007.7	14.5	975.3	1,044.8	1,016.6	16.3	953.8	1,045.4	1,007.7	20.6
7	980.1	1,034.6	1,016.9	15.7	973.3	1,046.7	1,013.0	17.9	982.0	1,046.0	1,019.2	12.2
8	987.7	1,036.1	1,017.0	12.0	985.9	1,029.4	1,007.4	7.3	975.4	1,038.6	1,012.7	13.8
9	971.4	1,023.6	1,001.7	14.6	980.3	1,045.2	1,014.6	15.1	984.4	1,032.0	1,013.0	7.3
10	963.8	1,035.7	1,016.5	16.5	977.0	1,042.1	1,021.7	11.1	975.8	1,047.5	1,023.0	11.1
11	961.7	1,029.4	1,015.5	14.4	970.4	1,042.0	1,004.2	15.1	969.2	1,035.2	1,016.5	13.1
12[a]	960.9	1,031.9	1,008.9	21.9	965.6	1,044.7	1,006.6	17.4	970.1	1,049.6	1,022.0	13.3
13	973.9	1,026.7	1,008.4	15.3	974.6	1,035.7	1,002.5	12.3	981.8	1,033.3	1,018.2	10.8
14	960.0	1,046.6	1,014.8	19.2	987.3	1,042.8	1,014.8	11.8	991.9	1,029.9	1,011.8	8.2
15	979.5	1,031.0	1,012.4	12.6	978.4	1,038.5	1,012.3	10.0	978.8	1,041.0	1,018.1	11.2
16[b]	967.8	1,029.9	1,011.5	15.7	968.6	1,034.4	1,009.0	14.4	970.0	1,035.9	1,002.4	13.5
17	979.4	1,038.1	1,014.4	16.8	975.1	1,040.8	1,013.1	15.1	983.0	1,045.3	1,013.5	13.3
18	985.5	1,036.8	1,016.0	14.2	973.6	1,036.3	1,012.3	13.0	968.7	1,045.6	1,010.3	17.2
19	970.7	1,032.2	1,011.0	18.1	955.3	1,044.7	1,009.7	18.5	975.1	1,043.4	1,006.4	14.7
20	983.9	1,028.2	1,007.3	13.5	971.6	1,037.8	1,011.6	17.0	978.9	1,038.7	1,011.6	12.6
21	974.7	1,036.6	1,020.6	15.2	978.7	1,040.1	1,014.1	13.0	960.9	1,038.2	1,000.1	16.8
22	970.5	1,033.0	1,011.6	17.1	988.7	1,043.2	1,014.2	10.1	972.1	1,026.1	1,006.2	11.7
23	966.3	1,031.9	1,010.8	15.1	991.7	1,032.4	1,014.8	10.9	973.0	1,044.0	1,014.3	15.7
24	969.2	1,037.0	1,008.7	16.9	971.8	1,033.6	1,004.8	12.3	994.2	1,023.5	1,011.0	5.8
25	992.3	1,030.6	1,019.0	7.8	998.6	1,032.0	1,015.1	7.2	956.1	1,077.3	1,018.1	17.1
26	987.4	1,034.7	1,016.0	12.4	994.3	1,026.7	1,014.7	5.4	965.2	1,070.5	1,010.4	12.3
27	971.6	1,027.6	1,007.7	15.2	999.6	1,032.7	1,017.1	6.2	996.0	1,037.5	1,014.4	7.8
28	971.7	1,030.3	1,010.3	14.7	967.6	1,046.0	1,010.2	16.8	974.5	1,039.5	1,009.7	15.9
29	992.6	1,029.5	1,014.0	9.3	958.0	1,038.3	1,007.4	16.7	967.8	1,046.1	1,011.2	16.9
30	967.3	1,031.4	1,012.8	16.9	958.6	1,047.3	1,018.0	17.4	974.4	1,042.3	1,018.5	13.9
Min (hPa)	960.0	1,023.6	1,001.7	7.8	955.3	1,026.7	1,002.5	5.4	953.8	1,023.5	1,000.1	5.8
Max (hPa)	992.6	1,046.6	1,020.6	21.9	999.6	1,047.3	1,021.7	18.5	996.0	1,077.3	1,023.0	20.6
Mean (hPa)	974.9	1,032.2	1,012.0	15.0	978.0	1,039.2	1,012.5	12.9	975.6	1,041.5	1,012.0	13.0
Stdev (hPa)	8.7	4.3	4.1	2.7	11.2	5.6	4.6	3.6	10.1	10.6	5.8	3.3

Also computed, similar values but for the composites. Note that the storms are not sorted in decreasing order of magnitude of mean sea level pressure

[a] Lothar windstorms

[b] Vivian windstorms

The atmosphere in the computational domain is characterised by a vertical component of the relative vorticity field that is positive (i.e., counter clockwise) in quadrants I and II and negative (i.e., clockwise) in quadrants III and IV, consistent with the p_{msl} and the geopotential fields. The relative vorticity is maximum to the west of the trough in the geopotential field, 2.87 day^{-1} at 825 hPa, located in the North Sea and minimum in the high pressure zone. Similar patterns are also found in the composites generated with HCGCM (1961–1990). In the vertical, the simulated relative vorticity profile increases upward in absolute values up to the 250 hPa level, reaching its maximum just below the jet. Figure 4c clearly shows the average positive values in quadrant I and II and negative values in quadrant III and IV

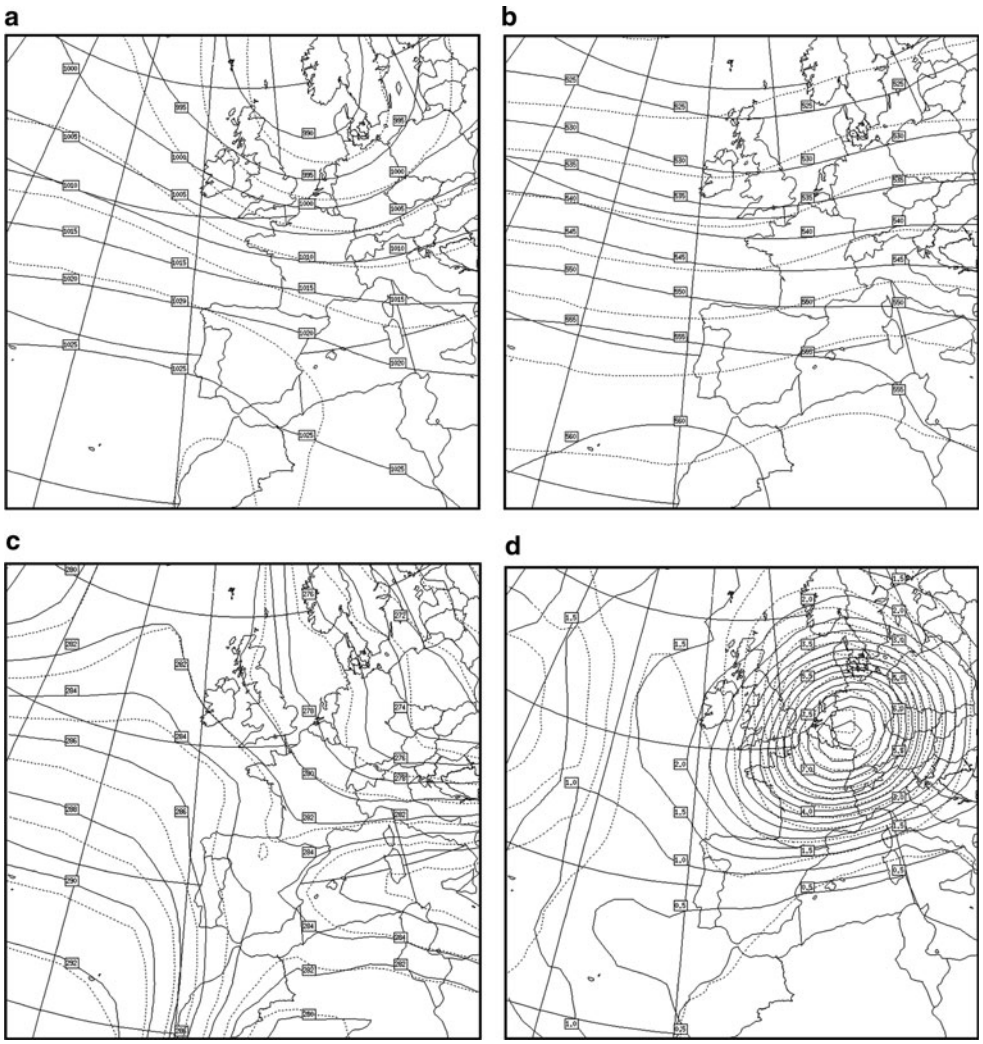

Fig. 3 Composite averages for current synoptic conditions conducive to strong winds over Switzerland. Each simulation (2×30) has been performed with the 150-km CRCM. The first composite average is generated on the basis of CRCM outputs driven by NCEP-NCAR reanalyses (*solid lines*) and the second by HCGCM GCM outputs for the period 1961–1990 (*dotted lines*); **a** p_{msl} in hPa with isobars drawn every 5 hPa; **b** 1,000–500 hPa thickness in dam with contour lines drawn every 5 dam; **c** surface temperature in K, isotherms drawn every 2K; **d** precipitation rate in mm day^{-1}, isoyets drawn every 0.5 mm day^{-1}

where a bias is noticed, compared to the composites generated with HCGCM (1961–1990).

The maximum Eady growth field is strong in a corridor 10° wide in a latitude centred on 50°N, and values reaching 3 day^{-1} at 900 hPa over Northern France and in the English Channel (not shown). Values are high over the ocean in the lowest levels off the cost of Brittany, at 3 day^{-1} at 950 hPa and increasing with height over the continent below 750 hPa, reaching again 3 day^{-1} over Germany and Switzerland at 875 hPa. In the vertical in quadrants I and II (Fig. 4d), the Eady growth rate profile is increasing sharply from the surface upward until the 900 hPa level is reached and has a secondary maximum at the 350 hPa level. Simulated profiles are similar to those observed but with a slight negative bias.

The vertical component of the baroclinicity vector (not shown) is characterised by a general dipole structure, where a positive contribution to the local tendency of the vertical component of the relative vorticity is found off the coast of the UK, France, and Spain over the Atlantic Ocean extending slightly inland to Switzerland reaching a maximum at 700 hPa, where it contributes to strengthening of cyclonic circulation, and a negative contribution located to the east of 10°E over continental areas above 40°N where it contributes negatively. A positive contribution to the cyclonic circulation is also diagnosed in the levels with pressure below 850 hPa over the Mediterranean Sea, reaching a maximum at 300 hPa. The general spatial pattern of this field is well captured by the simulated storm composite on average but may differ in the details. In the vertical, the profile is characterised by mostly positive values in quadrant I, negative values in quadrant II. As shown in Fig. 4e, the shape of the profile generally agrees compared to the composites generated with HCGCM (1961–1990).

The other main features include the divergence of the horizontal winds where a region of strong convergence at the 950 hPa level in a region centred over the Netherlands at 2.36 day^{-1}, consistent with the p_{msl} and the wind fields and a region of divergence aloft (350 hPa) at -1.31 day^{-1}.

Table 2 Linear correlation coefficients between composite mean fields generated by the 160-km CRCM driven by NCEP-NCAR and by HadAM3P (1961–1990)

Field	Spatial linear regression coefficients
p_{msl}	0.95
Φ (500)	0.94
P	0.81
T_{sfc}	0.95
v_H (1,000)	0.92
v_H (500)	0.96
v_H (250)	0.92
T(1,000)	0.95
T (350)	0.99
ζ (900)	0.88
ζ (250)	0.90
D_H (900)	0.68
D_H (250)	0.51
q (800)	0.86
σ_{BI} (900)	0.76
σ_{BI} (400)	0.85
N_z (950)	0.65
N_z (400)	0.60

Fields are the mean sea level pressure, p_{msl}; geopotential height field at 500 hPa Φ (500); precipitation P; the surface temperature; T_{sfc}, the horizontal wind speed component at 1,000, 500, and 250 hPa, v_H (1,000), v_H (500), v_H (250); the air temperature at 1,000 and 350 hPa, T (1000), T (350); the vertical component of the relative vorticity at 900 and 250 hPa, ζ (900), ζ (250); the divergence of the horizontal winds at 900 and 250 hPa, D_H (900), D_H (250); the specific humidity at 800 hPa, q (800); the maximum Eady growth rate at 900 and 400 hPa, σ_{BI}(900), σ_{BI}(400); and the vertical component of the baroclinicity vector at 950 and 400 hPa, N_z (950), N_z (400), respectively

In the vertical, the simulated divergence profile is similar to that observed, but with a positive shift mainly found over the ocean. The precipitation is consistent with the p_{msl} and the wind convergence fields. The specific humidity field is characterised by an important atmospheric moisture contribution coming from the warmer southern Atlantic Ocean (quadrant III) towards the interior of the continent (quadrant II). In the vertical, the simulated specific humidity profile is decreasing monotonically upward and is similar to that observed, but with a positive bias of 0.13 g kg^{-1} mainly found over land.

3.2 Expected future climate changes according to the SRES A2 scenario

The validation step has shown that the 30-storm composite means generated with HCGCM (1961–1990) reproduced many of the important features of the NCEP-NCAR synoptic conditions resulting in strong wind speeds over Switzerland. Therefore, this section analyses the synoptic conditions generating high winds over Switzerland during the period 2071–2100 under the IPCC SRES A2 scenario in terms of the composite mean fields, and compares the changes relative to the 1961–1990 period. The significance of the changes (i.e., differences between the two periods) has been initially calculated with a simple two-sided t test applied to the means; however, this test may not be suitable for evaluating the local significance of the differences as their distributions are often non-Gaussian. These have been complemented by non-parametric Mann–Whitney and Kolmogorov–Smirnov tests to verify if, on a grid-point basis, the whole distribution of these synoptic conditions is different or not.

The presentation of the composite mean changes follows a similar structure to that of Sect. 3.1. The mean sea level pressure change is up to 1 hp greater over the westernmost part of continental Europe, including the UK, but 3 hPa lower over the North Atlantic Ocean as well as over the Baltic Sea (not shown). Consequently, this is creating weaker west-east pressure gradients over a region centred over Ireland and extending roughly 5° to both the east and west, 10° in the southern and northern directions, and stronger pressure gradients over the Atlantic Ocean and over continental areas west of France, including Switzerland, Germany and Italy. The Kolmogorov–Smirnov and the Mann and Whitney tests seem to show that the distribution of the two p_{msl} composites in central western Europe, the UK, part of the North Atlantic and the Baltic Sea may be statistically different.

A tongue of high positive geopotential heights change at 500 hPa runs from the south Atlantic towards Ireland at the junction of quadrants I and II, with lesser change on both sides (Fig. 5a). This configuration creates a stronger east-west component of the geopotential height gradient, aligned with the coastal areas of Western Europe. The Mann and Whitney (Fig. 5a′) and the Kolmogorov–Smirnov tests indicate that the distribution of the two samples may be statistically different.

The 1,000 hPa temperature field changes indicate that a marked increase of up to 2°C over the North Atlantic Ocean and a much smaller increase over land (not shown); even a slight decrease over Southern Germany and Switzerland has been observed, thus producing a markedly sharp east-west temperature gradient along the European coastal areas. One remarkable feature appears in the vertical cross sections of the temperature differences shown in Fig. 7 where a very similar warming structure over the ocean around the 350 hPa level at more than 4°C in the South-North and in the West-East directions is diagnosed in the windstorm composites. The mean vertical profiles clearly indicate that the air temperature difference

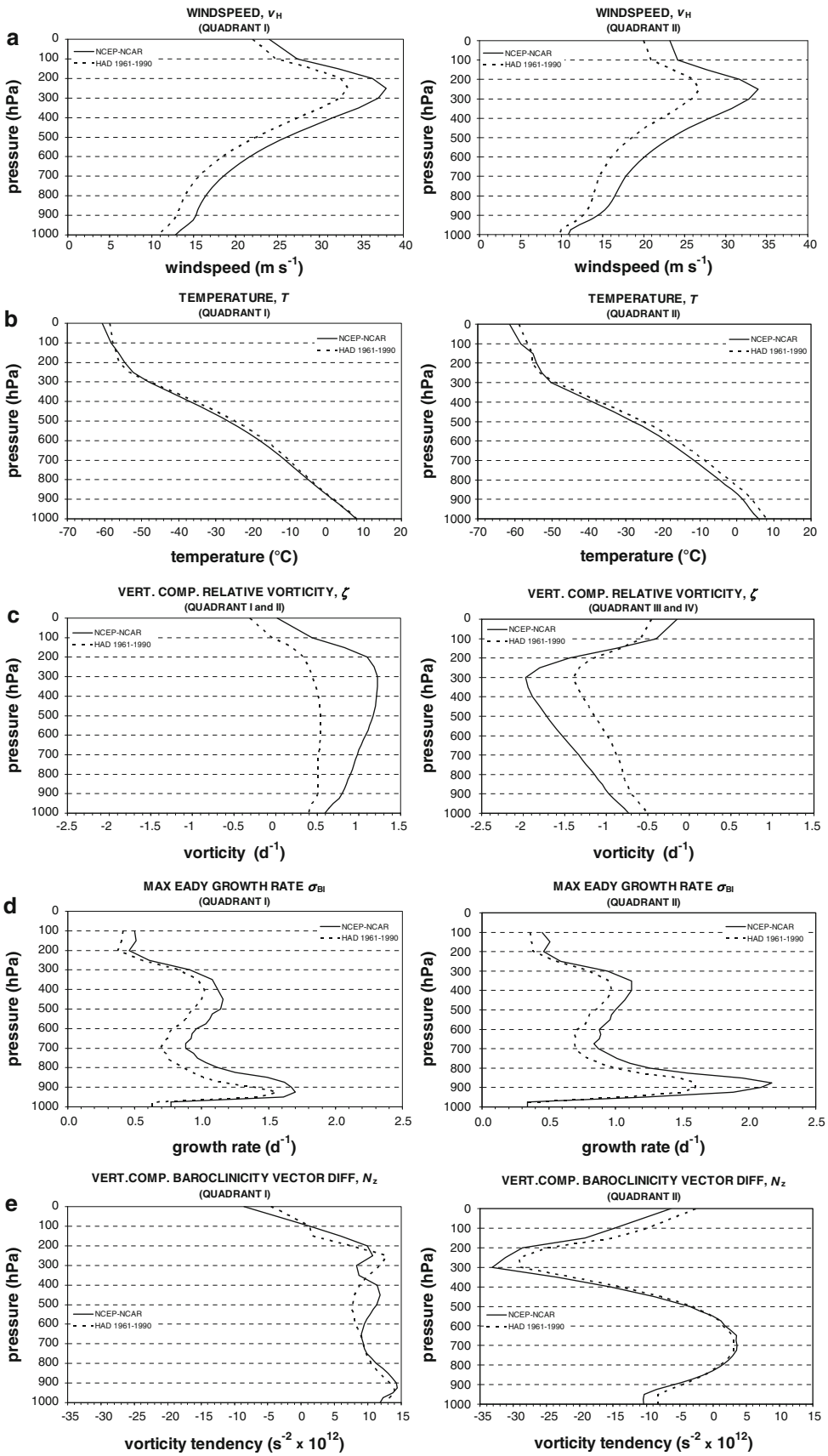

Fig. 4 Comparison of mean composite profiles for current storm-climate conditions averaged over individual quadrants where important features appear; **a** horizontal windspeed in m s^{-1}, **b** air temperature in °C; **c** vertical component of the relative vorticity in day^{-1}; **d** Eady growth rate maximum in day^{-1}; **e** vertical component of the baroclinicity vector in s^{-2} × 10^{12}. NCEP-NCAR profiles are in *bold lines*, those generated by HCGCM are in *dotted lines*

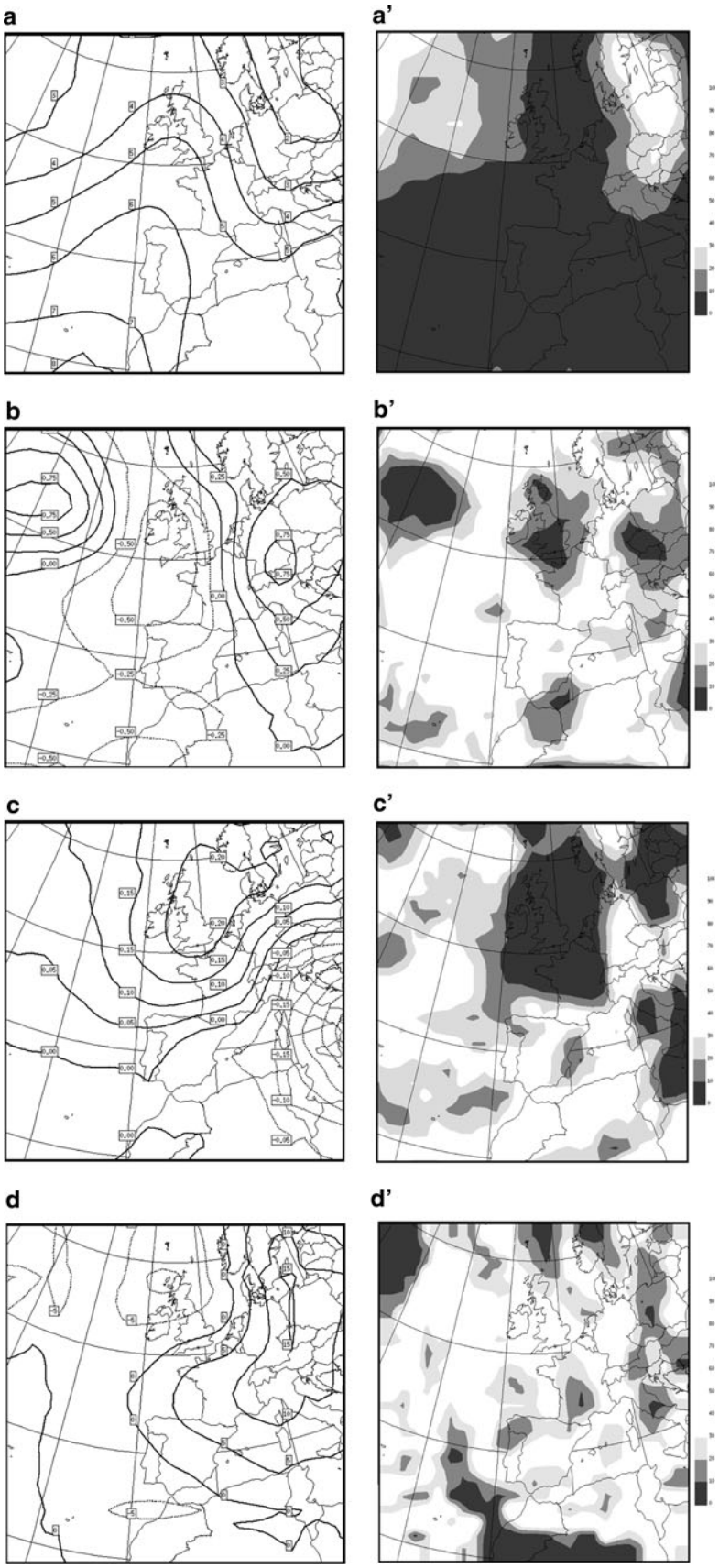

Fig. 5 Difference of composite averages between (2071–2100) under the SRES A2 warming scenario, and (1961–1990) periods on the *left*. On the *right*, the Mann–Whitney two-sample test giving the probability that these two samples are coming from the same distribution; on the graphs probability lower than 0.3 are in grey shades. **a** Geopotential heights at 500 hPa, contour lines drawn every 5 dm; **b** vertical component of the vorticity at 300 hPa, isolines drawn every 0.25 day^{-1}; **c** Eady growth rate maximum at 300 hPa, isolines drawn every 0.05 day^{-1}; **d** vertical component of the baroclinicity vector at 300 hPa, isolines drawn every 0.25 $s^{-2} \times 10^{12}$. In **b**–**d**, negative differences are in *dotted lines*

is positive in quadrant I with a maximum warming at the 400 hPa level, and less warming in quadrant II, particularly in the lower level over land (Fig. 6b). The Student's *t* test at 1,000 hPa indicates that the temperature change over the ocean and at altitude over the continent may be statistically significant. The same conclusions hold with the Mann and Whitney and the Kolmogorov–Smirnov tests (not shown).

The changes in the precipitation field averaged during these storms indicate a general increase of more than 4 mm day^{-1} on both sides of 50°N spreading in an 8° band (not shown). The maximum increase occurs in the secondary peak over the ocean in quadrant I, where more than 1.3 mm day^{-1} is expected, whereas there is less than a 1 mm day^{-1} enhancement in the main maximum of the 2071–2100 period. The Kolmogorov–Smirnov and the Mann and Whitney tests seem to indicate that the cumulative distribution function of the two precipitation sets may be statistically different in quadrant I.

The 1,000 hPa horizontal wind change is consistent with the change in the mean sea level pressure gradient (not shown). The sign and the phase of these changes are impacting in a similar fashion aloft up to the 650 hPa level (Fig. 6a). The winds at the 500 hPa level indicate no change of speed in the westernmost part of Europe and in the UK, but an increase of 2 m s^{-1} over the North Atlantic Ocean and a smaller increase west of France is noticeable, including Switzerland, Austria and neighbouring countries. The jet stream core diagnosed in Sect. 3.1 has shifted eastward. At altitudes above 300 hPa, the winds are stronger particularly over Northern France and over the UK. The differences of the mean vertical profiles indicate that there is practically no change of wind speeds in quadrant II below the 500 hPa level and an increase above it. In quadrant II, no change of wind speeds below 500 hPa level over the ocean and a decrease over land surfaces, and an increase above that level. The Kolmogorov–Smirnov and the Mann and Whitney tests (not shown) indicate that the cumulative distribution function of the two samples in central western Europe, the UK and some areas further north may be statistically different.

The changes in the vertical component of the relative vorticity field indicate a decrease over continental areas below 600 hPa and an increase over the North Atlantic at all levels, north of 45°N. Interestingly enough, the increase above 500 hPa tends to produce more positive vorticity west of 5°E (Fig. 5b). The differences of the mean vertical profiles clearly indicate that there is a general decrease of the relative vorticity over land below 650 hPa in quadrant I and an increase peaking at the 200 hPa level, and an increase over ocean in quadrant II at all levels (Fig. 6c). The Student's *t* test indicates that the vorticity change over land and over the ocean may be statistically significant. Similar conclusions hold with the Mann and Whitney (Fig. 5b′) and the Kolmogorov–Smirnov tests.

As shown in Fig. 5c, the difference in the Eady growth rate field indicate that the maximum rate of baroclinicity is increasing over the Atlantic Ocean in the levels below 850 hPa off the coast of Ireland in quadrant I at more than 0.3 day^{-1}, and decreasing over the coastal areas and further inland to the east in quadrant II. In the vertical, the Eady maximum baroclinicity profile increases over the ocean in quadrant I from the surface upward as far as 900 hPa, before decreasing and then further increasing at the 300 hPa level, as well as in quadrant II (Fig. 6d). The changes indicate however that there is a general decrease of this quantity below 400 hPa and an increase above that level in quadrant II. The Student's *t* test indications may be significant in regions of changes, as well as for the Mann and Whitney (Fig. 5c′) and the Kolmogorov–Smirnov tests.

The changes in the vertical component of the baroclinicity vector in the lowest levels show a significant reduction along the coastal areas and a positive contribution is located to the east of France, mainly above 50°N and over the North Atlantic Ocean (Fig. 5d). The vertical profiles show that there is a substantial increase of baroclinicity in quadrant II over land, particularly at the 300 hPa level, and a general decrease in quadrant I below the 400 hPa level (Fig. 6e). The Student's *t* test indications may be significant in regions of changes, as well as for the Mann and Whitney (Fig. 5d′) and the Kolmogorov–Smirnov tests.

The other main features that are not shown include changes in the divergence fields denoting less convergence over continental areas and more convergence in the Atlantic north of 50°N. The differences of the mean vertical profiles indicate that the divergence decreases from the surface layers to the 800 hPa level, then increases markedly up to the 300 hPa level. The changes in the specific humidity indicate a reduction of specific humidity over central Europe in the lower levels and more specific humidity above the 875 hPa level, over most of continental areas and over the North Atlantic Ocean, as well as over the Mediterranean Sea. The differences of the mean vertical profiles indicate that the average specific humidity increases everywhere at levels below 500 hPa over both oceanic areas. There is a positive change of moisture in the lowest levels, reaching a local maximum of 0.65 g kg^{-1} at 900 hPa, and then decreasing monotonically with height.

4 Discussion

The linear correlation coefficients in the computational domain between the mean of the 30-storm composites compiled on the basis of HCGCM outputs during the

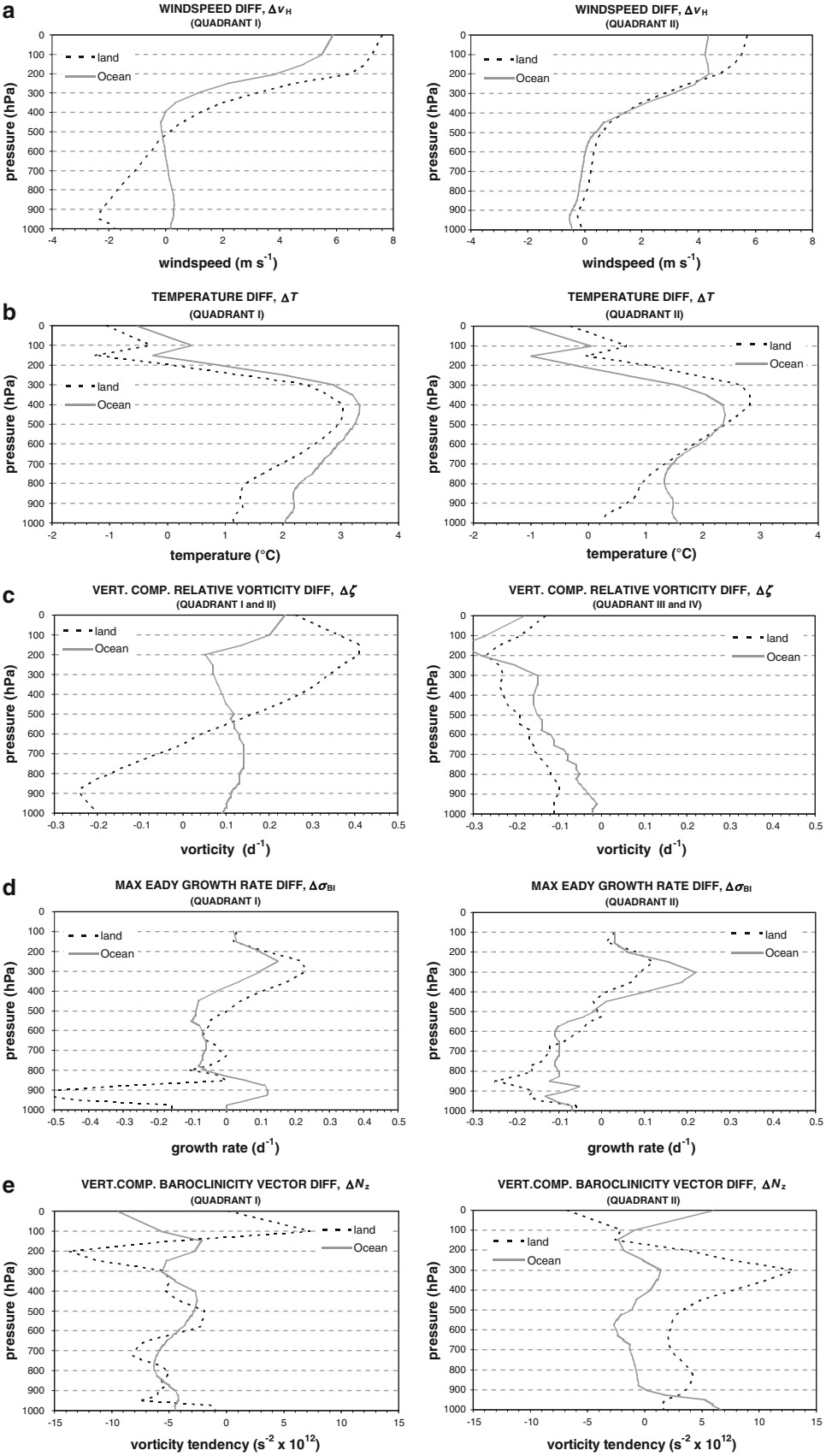

Fig. 6 Comparison of mean composite profile differences for 2071–2100 minus 1961–1990 storm-climate conditions averaged over individual quadrants where important features appear; **a** horizontal windspeed in m s^{-1}, **b** air temperature in °C; **c** vertical component of the relative vorticity in day^{-1}; **d** Eady growth rate maximum in day^{-1}; **e** vertical component of the baroclinicity vector in s^{-2} × 10^{12}. *Solid lines* represent ocean and *dotted lines* land profiles

period 1961–1990, and the mean of the 30-storm composite compiled on the basis of the NCEP-NCAR reanalysis, both downscaled by the Canadian RCM are generally above 0.6 on a grid-point basis (Table 2). The simulated synoptic patterns responsible for strong winds in Switzerland over the period 1961–1990 are found similar to a large extent with the observed ones (Fig. 3). This statement also holds true in the vertical plane as far as the vertical profiles of the storm composites averaged over the computational domain are concerned (Fig. 4).

The windstorms features shown above are consistent among variables and between vertical levels and, therefore, did not arise randomly from compositing (e.g., Fig. 2). The composite average of the mean sea level pressure found for the current climate is in line with the approximate location of the low centers responsible for considerable in the Swiss forests as shown in Schiesser et al. (1997; their Fig. 11). Then, scientific questions arise as to what extent the storm composite patterns are different from a climatological mean, and how far they can be assigned to storm occurrence through the analysis of the composites made out of "snapshots"? An examination of the synoptic conditions at the surface and aloft in the context of baroclinic instability follows. As shown in Fig. 3a the mean composite displays a low in the mean sea level pressure of about 986 and 990 hPa, respectively, for the NCEP-NCAR and the HCGCM (1961–1990), compared to 1,012 hPa on the computational domain average (see Table 1), which is considered as "intense" for wind storms induced by midlatitude cyclones in this part of the domain. When the upper-level flow fields are superimposed to the mean sea level pressure field, it is noticed, particularly along the 50°N, that cold temperature advection and warm temperature advection are associated with convergence to the West of 10°W longitude, thus to the West of the surface low, and divergence to the East of 0°E longitude, thus to the East of the surface low. In addition, the jet stream, diagnosed in the composite at 250 hPa along the 50°N, is having a high speed core flowing eastward at $v_H > 45$ m s^{-1}, or jet streak, of averaged speed of 48 m s^{-1} over Brittany that produces a region of confluence to the West of 10°W longitude at the jet entrance, and diffluence to the East of 5°E longitude at the exit, thus removing air above the surface low. The extension of the baroclinic instability theory to include latent heat release is also consistent in the composites: ascending air is diagnosed in the region of low-level convergence located over Western Germany, condensation occurs and latent heat release (amount to be quantified in a forthcoming study) which participate to strengthen the system, which produced the precipitation maximum over the borders of northeast France, southwest Germany and neighbouring countries as shown in Fig. 3d. Furthermore, the region of maximum vorticity of its eastern side has diverging air aloft, converging surface air, and ascending air motions, whereas on its western side, there is converging air aloft, diverging surface air, and descending air motions. A positive relative vorticity is also found south of the main low pressure centre and the highest winds are generally found to the north of the junction of the positive and negative relative vorticity values. However, the westward phase tilt of the upper level trough with height is modest. The description given above is valid for both set of composites produced by NCEP-NCAR reanalysis data and the HCGCM (1961–1990) outputs. Consequently, the flow fields in the composites for the current climate, as far as the baroclinic wave theory for developing cyclones along with some of its extension is concerned, are consistent.

Generally, the synoptic systems giving rise to wind storms in Switzerland look similar, in the first instance, during the period 2071–2100 simulated by HCGCM, on average, to the period 1961–1991. However, global warming imprints on these are an indication that they are recognised by statistically significant differences in the horizontal, as well as in the vertical, with the control period (Fig. 5). These are:

1. Mean sea level pressure is lower over the ocean in quadrants I and III, and higher in quadrants II and IV thus producing a pressure gradient that is stronger over the ocean off the coast of Ireland and over regions of northern Switzerland, but less over the coastal areas from the UK down to Spain.
2. A greater temperature contrast is noticeable between the Atlantic Ocean and Mediterranean Sea than the cooler surface of the European continent at low levels. Greater differences (>4°C) are found in the higher atmosphere over the ocean and less in the lower levels over land. The thickening of geopotential surfaces over the ocean compared to a lesser thickening over the continent (Fig. 5a) seems to foster the development of storms over Switzerland by fostering the advection of cold air over the continent. Interestingly enough, the structure of the temperature change in the South-North and in the West-East directions in the mid-latitudes (Fig. 7) are both characterized by a 4°C warming at the 400 hPa level and less below. If the signature of the atmospheric warming when climate changes is found the same in both, then the finding tends to corroborate the Houghton (2005) hypothesis that storm activity in a warmer world may increase in response to larger land-sea temperature contrasts. Other remarkable features include the combination of the particular temperature change in the West-East direction at 400 hPa around 50°N, with the increase of the vertical component of

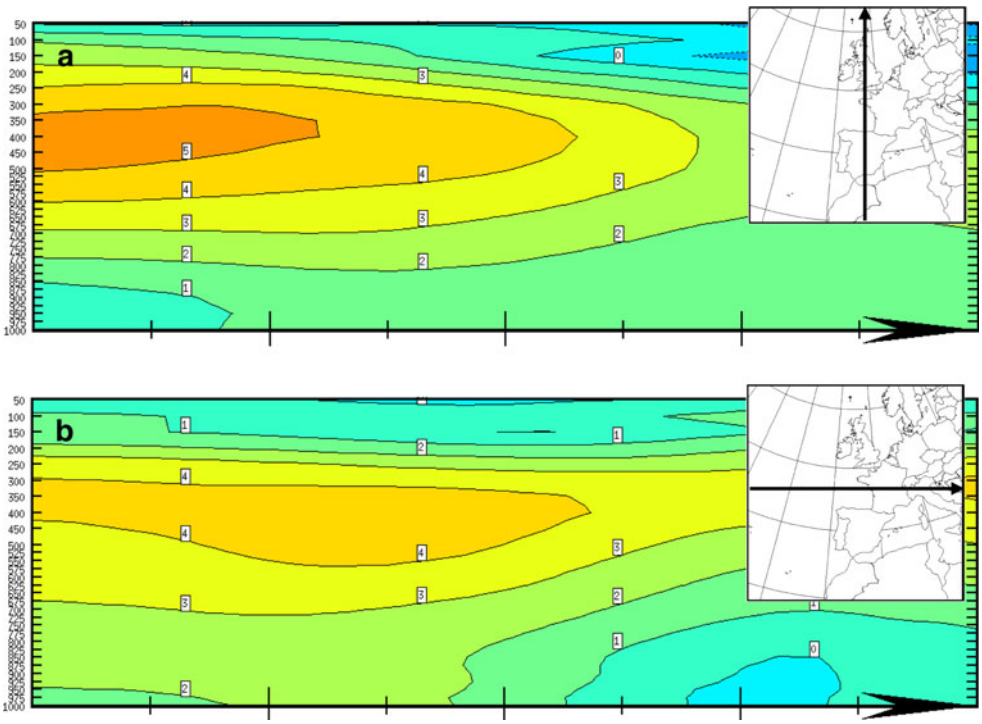

Fig. 7 Vertical cross sections of the temperature differences (°C) between the 2071–2100 and the 1961–1990 periods as generated by the HCGCM GCM in the South-North direction (**a**) and in the West-East direction (**b**) as shown in the inserts

the relative vorticity over land as well as that of the vertical component of the baroclinicity vector, that of the maximum Eady growth rate at the same level and latitude, and of the eastward extension of the jet stream core. Potential temperature profiles also suggest that a more stable atmosphere (i.e., differences increase with altitude) would contribute to the generation of more wind gusts at the surface.

3. Remarkable features are taking place in a general opposite fashion in the northern quadrants of the domain. Differences in quadrant I indicate higher surface and air temperatures, higher windspeed above 400 hPa, stronger vertical component of the relative vorticity from the surface aloft, increase of the Eady growth maximum in the 1,000–950 hPa layer, and a decreases in the 800–400 hPa layer, weaker vertical component of the baroclinicity vector from the surface aloft, increase of atmospheric specific humidity is simulated (up to 0.7 g kg^{-1}) below 400 hPa, whereas differences in quadrant II indicate decrease in surface temperatures and small changes in air temperatures below 400 hPa, little changes in windspeed below 400 hPa, decrease in the vertical component of the relative vorticity from the surface aloft, the Eady growth maximum decreases below 400 hPa, stronger vertical component of the baroclinicity vector from the surface aloft, and a decrease of atmospheric specific humidity (up to 0.5 g kg^{-1}) below 900 hPa.

It has been noticed in earlier studies (e.g., Schubert et al. 1998) that in a 2× CO_2 experiment with GCMs, storm track intensifies at the eastward end, whereas the cyclone frequency shifts northeastward. In addition, no increase of the cyclone frequency in the eastern part of the North Atlantic (where the storm track anomaly has its maximum) was detected. In this paper, many synoptic features found in the "simulated" storm composites undergo a westward shift in the low levels (i.e., from quadrant II to quadrant I) when climate warms according to the IPCC SRES A2 emission scenario. A decrease in the mean sea level pressure, an increase of the vertical component of the relative vorticity, an increase of the Eady growth maximum in the low levels, and an increase in precipitation were found. At the same time, more subtle changes occur aloft: the North-South component of the temperature gradient increase in the upper levels and it remains nearly constant in the lower levels, while the East-West component increases in the upper levels and much less in the low levels. The net result is towards a greater temperature contrast between the relatively warm North Atlantic Ocean and the colder continental surfaces. Also, the vertical component of the baroclinicity vector indicates a positive contribution of the vorticity tendency over the warmer ocean (quadrant III) and a negative contribution over the coastal areas and over the northern North Atlantic (Fig. 6e). Thus, the increase of the vertical component of the relative vorticity in quadrant I is not due to the contribution of the baroclinicity vector;

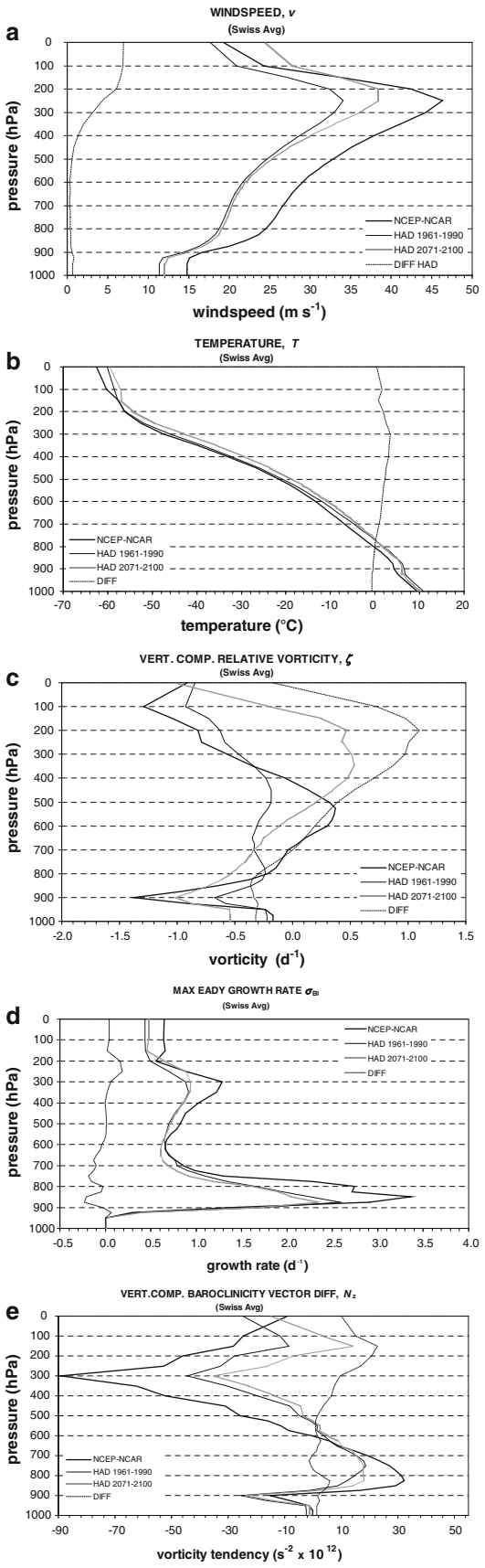

Fig. 8 Comparison of composite profile means and differences over Switzerland as generated by the 160-km CRCM driven by the NCEP-NCAR reanalysis and by the HCGCM GCM; **a** horizontal windspeed in m s^{-1}, **b** air temperature in °C; **c** vertical component of the relative vorticity in day^{-1}; **d** Eady growth rate maximum in day^{-1}; **e** vertical component of the baroclinicity vector in $s^{-2} \times 10^{12}$ ▶

the influence of diabatic heating is presumably playing a role as can be seen in the moisture field differences (not shown).

Northern hemisphere winter storm tracks have been diagnosed using σ_{BI} at 700 hPa, ζ at 850 and at 500 hPa in Greeves et al. (2007), Carnell and Senior (1998) used σ_{BI} at 500 hPa, Bengtsson et al. (2006) used ζ at 850 hPa. Our results have shown that the magnitude of Eady growth maximum and its differences between the periods 2071–2100 and 1961–1990 are greater in the layer around the 900 hPa level and lesser at 700 hPa. Consequently, σ_{BI} at 700 hPa is not an appropriate measure to diagnose the synoptic conditions fostering windstorms over Switzerland; neither does σ_{BI} at 500 hPa. However, ζ at 850 and at 500 hPa, as well as their differences are providing for useful information about the storms at these levels. Some others, such as Pinto et al. (2007), used a variety of methods including σ_{BI} at 400 hPa, which seems in this case to be a better candidate (Fig. 6d). The above findings are also in line with the analysis of Raible (2007) who stated that, among other processes, the land–sea temperature contrast plays a role to generate extremes in cyclone intensity.

Over Switzerland, the profiles of the composite averages and differences between the (2071–2100) and (1961–1990) are in many points similar to those averaged over quadrant II (see Fig. 1). The simulated windspeed over Switzerland shows a hint of a low-level jet at 850 hPa, and the strongest winds flowing above at the Eastern margin of the jet stream is found at 250 hPa. The differences indicate no changes below 500 hPa but an enhancement of the winds of 5 m s^{-1} at the level of the jet stream (Fig. 8a). The temperature profile differences indicate that for these windstorms as climate warms, the static stability is increased where a slight cooling of the air is simulated near the surface and a warming above 750 hPa reaching its maximum at 300 hPa (Fig. 8b). The vertical component of the relative vorticity shows a slight decrease in the lowest level, but an intensification especially in the 500–150 hPa levels where it become much more cyclonic (Fig. 8c). The maximum Eady growth rate shows similar changes where it decreases slightly in the lowest levels and increases around 250 hPa (Fig. 8d). The vertical component of the baroclinicity vector indicates general positive differences throughout the profile, but more pronounced around the 250 hPa level (Fig. 8e).

5 Conclusions

This paper is aimed at studying the synoptic conditions fostering high winds over Swiss territory for the current climate and compares these to those for future climate projections in a global climate warming scenario. A method for analysing synoptic conditions conducive to windstorms over a limited domain using composites is thus proposed. Although the analysis was not aimed at investigating the change of wind speeds and directions when climate changes, local winds from the identification procedure did not show any significant change in Switzerland regarding the mean speeds. However, more north-westerly flows with global warming were found in the 30 most intense windstorm composites over the period 2071–2100, and this is in line with the findings of Beniston et al. (2007). As noticed in other studies (e.g., Pinto et al. 2007), and in line with the results shown above, despite the little change in the mean cyclone intensities by the end of the twenty-first century, alterations are prominent over the Eastern North Atlantic and Western Europe. This also fits with the findings of Trigo (2006) showing that extreme Atlantic cyclone events tend to travel in the eastern part of the North Atlantic; also, Hall et al. (1994) found an increase in the kinetic energy downstream of the storm tracks in the northeast North Atlantic.

The proposed method of compiling atmospheric conditions on the basis of selected windstorms identified on a local basis, and of compositing storm statistics, contributes in the analysis of the synoptic conditions of extreme windstorms over Switzerland. The different average values computed from the composites based on NCEP-NCAR reanalysis have been shown to be realistically reproduced these by the HCGCM over the period 1961–1990. When compared to the observed climatology from the months of October to March, the signature of the composite storms over Switzerland is characterised by a westward shift for many of the field features.

The synoptic conditions producing high surface winds in Switzerland for the period 2071–2100 are qualitatively similar to those for the period 1961–1990. However, the analysis of the differences in the 30-year storm composites has shown subtle changes in the synoptic fields associated with windstorms. There is a stronger positive temperature change in the atmosphere over the ocean to the South of the computational domain than in the North and over the continent. Baroclinicity is strongly modified with altitude, but also as a function of the configuration of the ocean and continent, so that windstorms in the warmer climate scenario take advantage of a situation in which a warmer Atlantic Ocean is combined with a colder surfaces on the fringe of the western European continent. Atmospheric moisture seems also to play an important role in the evolution of the baroclinic wave. This role will be determined in a forthcoming study. The analyses carried out above should be critically assessed in view of the fact that the ensuing conclusions are based on a single GCM outputs (HCGCM); consequently, other driving models should be envisaged to reinforce these.

The differences in the distribution of the flow fields and other related variables of these thirty storm composites simulated by the Hadley GCM over the two periods 1961–1990 and 2071–2100 have been shown to be consistent with each other. However, differences in the storm composites are not correlated with the mean changes of global climate warming on average. Thus, one may not use the latter to infer the potential behaviour of windstorms over Switzerland. Since those cyclones responsible for strong wind in Switzerland considered in this study are presumably a subset of all extreme cyclones examined in others (i.e., Leckebusch et al. 2006; Leckebusch and Ulbrich 2004), the comparison between results obtained here and the latter is a rather delicate exercise. As stated in the paper by Leckebusch et al. (2006) on the basis of GCMs simulated outputs, winter cyclones in the North Atlantic are a principal cause of the occurrence of extreme, damage-causing wind speeds. When all systems are considered, a common feature of all investigated GCMs is a reduced track density over central Europe under climate change conditions. If only extreme cyclones are taken into account, and an increasing cyclone activity for western parts of central. However, the climate change signal reveals a reduced spatial coherency when compared to all systems, where changes (windspeed intensity and frequency, location and extension of the affected areas, and level of changes), are shown to be highly dependent on the driving GCM, whereas differences between RCMs when driven by the same GCM are relatively small. In spite of this, as stated above, the different average values analysed in the "observed" composite reproduced realistically these of the HCGCM over the period 1961–1990. Consequently, this retained much attention and paved the way to further analyses as described in this paper.

This study has contributed to support the hypothesis suggested by Houghton (2005) that storminess in a warmer world increases in response to larger land-sea temperature contrasts. Warming is stronger over the Atlantic Ocean and less over the continent, where there are cooling conditions in the lowest atmospheric level of southern Germany and over the tropical mid troposphere, than it does over the polar atmosphere.

Although the dynamical consequences of global warming are not as marked as the thermodynamical changes, the structures of the flow in a warmer world take advantage of the altered thermodynamic structures in the atmosphere so as to produce a comparable number of stormy weather

conditions over continental Europe, and in Switzerland in particular. This is not in contradiction with the earlier large-scale analysis carried out by Boer (1995) who stated that the net poleward transport of energy by the atmosphere is remarkably unchanged when climate warms. That the same amount of energy is transported by a generally less active atmosphere shows that, in a sense, the flow structures are more "efficient" in a warmer climate.

In order to obtain a deeper understanding of the mechanisms driving these current and future storms, it is planned in a forthcoming study to use some diagnostic software especially designed to analyse, interpret and understand numerical model outputs called "Dionysos" (Caron et al. 2005). It includes a complete set of diagnostic equations and enables to separate quantitatively different physical and dynamical process in several important meteorological fields. This will help us to better understand how these storms are generated and maintained and, further, how they produce high winds at the surface when the climate is warming. Especially, the role of the sensible and latent heat, as mentioned in Wernli et al. (2002) as an important process during the December 1999 Lothar storm for example, as well as temperature and vorticity advection in the evolution of such baroclinic waves will be investigated.

Finally, it must be emphasised that the methodology described above is also applicable to other extreme events, such as heavy precipitation. A preliminary analysis of an ongoing project has been carried out to identify the synoptic conditions conducive to heavy precipitation in Switzerland. The role of the water temperature in the Mediterranean Sea, coupled with south-westerly atmospheric circulation, has been recognised as playing a key role, thus helping to demonstrate that this method may produce other, promising results.

Acknowledgments The work reported in this paper is based on discussions during meetings of the EU PRUDENCE and ENSEMBLES projects that have been very useful in formulating the ideas and concepts discussed here. I would also like to thank two anonymous reviewers for their insightful comments which helped improve the manuscript. I finally thank the climate modelling team of ESCER at Montréal who developed and provide the CRCM used in this study.

References

Alexandersson H, Tuomenvirta H, Schmith T, Iden K (2000) Trends of storms in NW Europe derived from an updated pressure data set. Clim Res 14:71–73

Bärring L, von Storch H (2004) Northern European Storminess since about 1800. Geophys Res Lett 31:L20202. doi:10.1029/2004GL020441

Bengtsson L, Hodges KI, Roeckner E (2006) Storm tracks and climate change. J Clim 19:3518–3543

Bengtsson L, Hodges KI, Keenlyside N (2009) Will extratropical storms intensify in a warmer climate? J Clim 22:2276–2301

Beniston M, Stephenson DB, Christensen OB, Ferro CAT, Frei C, Goyette S, Halsnaes K, Holt T, Jacob D, Jylhä K, Koffi B, Palutikof J, Schöll R, Semmler T, Woth K (2007) Future extreme events in European climate: an exploration of Regional Climate Model projections. Clim Change 81:71–95. doi:10.1007/s10584-006-9226-z

Biner S, Caya D, Laprise R, Spacek L (2000) Nesting of RCMs by imposing large scales. In: Research activities in atmospheric and oceanic modelling, WMO/TD-No. 987, Report No. 30, 2000, pp 7-3–7-4

Blackmon ML (1976) A climatological spectral study of the 500-mb geopotential height of the Northern Hemisphere wintertime circulation. J Atmos Sci 33:1607–1623

Boer GJ (1995) Some dynamical consequences of greenhouse gas warming. Atmos Ocean 33:731–751

Branscome LE, Gutowski WJ (1992) The impact of doubled CO_2 on the energetics and hydrologic processes of mid-latitude transient eddies. Clime Dyn 8:29–37

Carnell RE, Senior CA (1998) Changes in mid-latitude variability due to increasing greenhouse gases and sulphate aerosols. Clim Dyn 5:369–383. doi:10.1007/s003820050229

Caron J-F, Zwack P, Pagé C, cited (2005): DIONYSOS: A diagnostic tool for numerically-simulated weather systems. http://www.dionysos.uqam.ca/documentation_e.html

Caya D, Laprise R (1999) A semi-implicit semi Lagrangian regional climate model: the Canadian RCM. Mon Weather Rev 127:341–362

Chang EKM, Song S (2006) The seasonal cycles in the distribution of precipitation around cyclones in the Western North Pacific and Atlantic. J Atmos Sci 63:815–839. doi:10.1175/JAS3661.1

Chang EKM, Lee S, Swanson KL (2002) Storm tracks dynamics. J Clim 15:2163–2183

Christensen JH, Carter TR, Giorgi F (2002) PRUDENCE employs new methods to assess European climate change. EOS 83:147

Della-Marta PM, Pinto JG (2009) Statistical uncertainty of changes in winter storms over the North Atlantic and Europe in an ensemble of transient climate simulations. Geophys Res Lett 36:L14703. doi:10.1029/2009GL038557

Fink AH, Brücher T, Ermert E, Krüger A, Pinto JG (2009) The European storm Kyrill in January 2007: Synoptic evolution, meteorological impacts and some considerations with respect to climate change. Nat Hazards Earth Syst Sci 9:405–423

Fischer-Bruns I, von Storch H, González-Rouco JF, Zorita E (2005) Modelling the variability of midlatitude storm activity on decadal to century time scales. Clim Dyn 25:461–476

Fuhrer J, Beniston M, Fischlin Ch A, Goyette Frei S, Jasper K, Pfister C (2006) Climate risks and their impact on agriculture and forests in Switzerland. Clim Change 79:79–102. doi:10.1007/s10584-006-9106-6

Gitelman A, Risbey J, Kass R, Rosen R (1997) Trends in the surface meridional temperature gradient. Geophys Res Lett 24:1243–1246

Goyette S (2008) Development of a model-based high resolution extreme surface wind climatology for Switzerland. Nat Hazards 44:329–339. doi:10.1007/s11069-007-9130-5

Goyette S, Beniston M, Caya D, Laprise JPR, Jungo P (2001) Numerical investigation of an extreme storm with the Canadian Regional Climate Model : The case study of windstorm VIVIAN, Switzerland, February 27, 1990. Clim Dyn 18:145–178

Goyette S, Brasseur O, Beniston M (2003) Application of a new wind gust parameterisation. Multi-scale case studies performed with the Canadian RCM. J Geophys Res 108(D13):4374–4390

Greeves CZ, Pope VD, Stratton RA, Martin GM (2007) Representation of Northern Hemisphere winter storm tracks in climate models. Clim Dyn 28:683–702

Gulev SK, Zolina O, Grigoriev S (2001) Extratropical cyclone variability in the Northern Hemisphere winter from the NCEP/NCAR reanalysis data. Clim Dyn 17:795–809

Hall N, Hopkins B, Valdes P, Senior CA (1994) Storm tracks in a high-resolution GCM with doubled carbon dioxide. Q J Roy Meteorol Soc 120:1209–1230. doi:10.1002/qj.49712051905

Held IM (1993) Large-scale dynamics and global warming. Bull Am Meteorol Soc 74:228–241

Heneka P, Hofherr T, Ruck B, Kottmeier C (2006) Winter storm risk of residential structures—model development and application to the German state of Baden-Württemberg. Nat Hazards Earth Syst Sci 6:721–733

Holton JR (2004) An introduction to dynamic meteorology. International geophysics series, 4th edn. Academic Press (Elsevier), New York, 535 pp

Hoskins B, Valdes PJ (1990) On the existence of storm tracks. J Atmos Sci 47:1854–1864

Houghton JT (2005) Global warming. Rep Prog Phys 68:1343–1403. doi:10.1088/0034-4885/68/6/R02

Iskenderian H, Rosen R (2000) Low-frequency signals in midtropospheric submonthly temperature variance. J Climate 13:2323–2333

Kalnay E et al (1996) The NCEP/NCAR 40-years reanalysis project. Bull Am. Meteorol Soc 77:437–471

Knippertz P, Ulbrich U, Speth P (2000) Changing cyclones and surface wind speeds over the North Atlantic and Europe in a transient GHG experiment. Clim Res 15:109–122

Kunkel KE, Pielke RA, Changnon S A Jr (1999) Temporal fluctuations in weather and climate extremes that cause economic and human health impacts: a review. Bull Am. Meteorol Soc 80:1077–1098

Lambert SJ, Fyfe JC (2006) Changes in winter cyclone frequencies and strengths simulated in enhanced greenhouse warming experiments: Results from the models participating in the IPCC diagnostic exercise. Clim Dyn 26:713–728

Lambert S, Sheng J, Boyle J (2002) Winter cyclone frequencies in thirteen models participating in the Atmospheric Model Intercomparison Project (AMIP 1). Clim Dyn 19:1–16

Land C, Feichter J (2003) Stratosphere-troposphere exchange in a changing climate simulated with the general circulation model MAECHAM4. J Geophys Res 108:8523

Laprise R, Caya D, Bergeron G, Giguère M (1997) The formulation of the André Robert MC2 (mesoscale compressible community) model. Atmos Ocean 35:195–220

Laprise R, Caya D, Giguere M, Bergeron G, Côté H, Blanchet J-P, Boer GJ, McFarlane NA (1998) Climate and climate change in Western Canada as simulated by the canadian regional climate model. Atmos Ocean 36:119–167

Leckebusch GC, Ulbrich U (2004) On the relationship between cyclones and extreme windstorm events over Europe under climate change. Glob Planet Change 44:181–193

Leckebusch G, Koffi B, Ulbrich U, Pinto J, Spangehl T, Zacharias S (2006) Analysis of frequency and intensity of European winter storm events from a multi-model perspective, at synoptic and regional scales. Clim Res 31:59–74

Lindzen RS, Farrell B (1980) A simple approximation result for the maximum growth rate of baroclinic instabilities. J Atmos Sci 37:1648–1654

Lionello P, Boldrin U, Giorgi F (2008) Future changes in cyclone climatology over Europe as inferred from a regional climate simulation. Clim Dyn 30:657–671. doi:10.1007/s00382-007-0315-0

Löptien U, Zolina O, Gulev S, Latif M, Soloviov V (2008) Cyclone life cycle characteristics over the Northern Hemisphere in coupled GCMs. Clim Dyn 31:507–532. doi:10.1007/s00382-007-0355-5

McFarlane NA, Boer GJ, Blanchet J-P, Lazare M (1992) The Canadian climate centre second generation general circulation model and its equilibrium climate. J Clim 5:1013–1044

Munich Re (1999) Topics 2000—natural catastrophes—the current position, Munich, pp 126. http://www.munichre.com

Nakićenović N et al (2000) IPCC special report on emissions scenarios. Cambridge University Press, Cambridge 599 pp

Nielsen JW, Dole RM (1992) A survey of extratropical cyclone characteristics during GALE. Mon Weather Rev 120:1156–1168

Osborn TJ, Briffa KR, Tett SFB, Jones PD, Trigo RM (1999) Evaluation of the North Atlantic Oscillation as simulated by a coupled climate model. Clim Dyn 15:685–702

Paciorek C, Risbey J, Ventura V, Rosen R (2002) Multiple indices of Northern Hemisphere cyclone activity, winters 1949–1999. J Clim 15:1573–1590

Peixoto JP, Oort AH (1991) Physics of climate. American Institute of Physics, New York 520 pp

Pinto JG, Ulbrich U, Leckebusch GC, Spangehl T, Reyers M, Zacharias S (2007) Changes in storm track and cyclone activity in three SRES ensemble experiments with the ECHAM5/MPI-OM1 GCM. Clim Dyn 29:195–210

Pinto JG, Zacharias S, Fink AH, Leckebusch GC, Ulbrich U (2009) Factors contributing to the development of extreme North Atlantic cyclones and their relationship with the NAO. Clim Dyn 32:711–737. doi:10.1007/s00382-008-0396-4

Pope DV, Gallani M, Rowntree R, Stratton A (2000) The impact of new physical parameterizations in the Hadley Centre climate model HadAM3. Clim Dyn 16:123–146

Raible CC (2007) On the relation between extremes of midlatitude cyclones and the atmospheric circulation using ERA40. Geophys Res Lett 34:L07703. doi:10.1029/2006GL029084

Raible CC, Yoshimori M, Stocker TF, Casty C (2007) Extreme midlatitude cyclones and their implications for precipitation and wind speed extremes in simulations of the Maunder Minimum versus present day conditions. Clim Dyn 28:409–423

Raible CC, Della-Marta PM, Schwierz C, Wernli H, Blender R (2008) Northern hemisphere midlatitude cyclones: a comparison of detection and tracking methods and different reanalyses. Mon Weather Rev 136:880–897

Rockel B, Woth K (2007) Extremes of near-surface wind speed over Europe and their future changes as estimated from an ensemble of RCM simulations. Clim Change 81:267–280

Roebber PJ (1984) Statistical analysis and updated climatology of explosive cyclones. Mon Weather Rev 112:1577–1589

Rolfson DM, Smith PJ (1996) A composite diagnosis of synoptic-scale extratropical cyclone development over the United States. Mon Weather Rev 124:1084–1099

Rudeva I, Gulev SK (2007) Climatology of cyclone size characteristics and their changes during the cyclone life cycle. Mon Weather Rev 135:2568–2587

Sanders F, Gyakum JR (1980) Synoptic-dynamic climatology of the "Bomb". Mon Weather Rev 108:1589–1606

Schiesser HH, Pfister C, Bader J (1997) Winter storms in Switzerland north of the alps 1864/1865–1993/1994. Theor Appl Climatol 58:1–19

Schinke H (1993) On the occurence of deep cyclones over Europe and the North Atlantic in the period 1930–1991. Beitr Phys Atmos 66:223–237

Schmith T, Kaas E, Li T-S (1998) Northeast Atlantic winter storminess 1875–1995 re-analysed. Clim Dyn 14:529–536

Schubert M, Perlwitz J, Blender R, Fraedrich K, Lunkeit F (1998) North Atlantic cyclones in CO_2-induced warm climate simulations: frequency, intensity, and tracks. Clim Dyn 14:827–837

Schüepp M, Schiesser HH, Huntrieser H, Scherrer HU, Schmidtke H (1994) The winterstorm "VIVIAN" of 27 February 1990: about the meteorological development, wind forces and damage situation in the forests of Switzerland. Theor Appl Climatol 49:183–200

Serreze MC (1995) Climatological aspects of cyclone development and decay in the arctic. Atmos Ocean 33:1–23

Stephenson DB, Wanner H, Broennimann S, Luterbacher J (2002) The History of Scientific Research on the North Atlantic Oscillation. In: Hurrell JW, Kushnir Y, Ottersen G, Visbeck M (eds) The North Atlantic Oscillation: climatic significance and environmental impact. Geophysical Monograph 134, American Geophysical Union, Washington, pp 37–50

Stephenson DB, Pavan V, Collins M, Junge MM, Quadrelli R et al (2006) North Atlantic Oscillation response to transient greenhouse gas forcing and the impact on European winter climate: a CMIP2 multi-model assessment. Clim. Dyn. 27:401–420

Tanguay M, Robert A, Laprise R (1990) A semi-implicit semi-Lagrangian fully compressible regional forecast model. Mon Weather Rev 118:1970–1980

Taylor KE, Williamson D, Zwiers F (2000) The sea surface temperature and sea-ice concentration. PCMDI Rep. No 60, Lawrence Livermore Nat. Lab, California, USA, 2000, 24 pp

Trigo IF (2006) Climatology and interannual variability of storm-tracks in the Euro-Atlantic sector: a comparison between ERA-40 and NCEP/NCAR reanalyses. Clim Dyn 26:127–143

Ulbrich U, Christoph M (1999) A shift of the NAO and increasing storm track activity over Europe due to anthropogenic greenhouse gas forcing. Clim Dyn 15:551–559

Ulbrich U, Fink AH, Klawa M, Pinto JG (2001) Three extreme storms over Europe in December 1999. Weather 56:70–80

Ulbrich U, Leckebusch GC, Pinto JG (2009) Cyclones in the present and future climate: a review. Theor Appl Climatol 96:117–131. doi:10.1007/s00704-008-0083-8

von Storch H, Weisse R (2008) Regional storm climate and related marine hazards in the Northeast Atlantic. In: Diaz HF, Murnane RJ (eds) Climate extremes and society, Cambridge. Cambridge University Press, Cambridge 340 pp

Wang XL, Swail VR, Zwiers FW (2006) Climatology and changes of extratropical storm tracks and cyclone activity: comparison of ERA-40 with NCEP/NCAR Reanalysis for 1958–2001. J Clim 19:3145–3166

Wang XL, Zwiers FW, Swail VR, Feng Y (2009) Trends and variability of storminess in the Northeast Atlantic Region, 1874–2007. Clim Dyn 33:1179–1195. doi:10.1007/s00382-008-0504-5

WASA Group (1998) Changing waves and storms in the Northeast Atlantic. Bull Am Meteorol Soc 79:741–760

Weisse R, von Storch H, Feser F (2005) Northeast Atlantic and North Sea storminess as simulated by a Regional Climate Model during 1958–2001 and comparison with observations. J Clim 18:465–479

Wernli H, Dirren S, Liniger MA, Zillig M (2002) Dynamical aspects of the life cycle of the winter storm "Lothar" (24–26 December 1999). Q J Roy Meteorol Soc 128:405–429

Wilks DS (2006) Statistical methods in the atmospheric science. International geophysics series, vol 91, 2nd edn. Elsevier/Academic Press, Amsterdam/London 627 pp

Wilson MF, Henderson-Sellers A (1985) A global archive of land cover and soils data for use in general circulation climate models. J Climatol 5:119–143

Woodworth P, Blackman D (2002) Changes in extreme high waters at Liverpool since 1768. Int J Climatol 22:697–714

Zwack P, Okossi B (1986) A new method for solving the quasigeostrophic omega equation by incorporating surface pressure tendency data. Mon Weather Rev 114:655–666

Zwiers FW, Kharin VV (1998) Changes in the extremes of the climate simulated by CCC GCM2 under CO^2 doubling. J Clim 11:2200–2222